VERSITA

OPTO-ELECTRONICS REVIEW **20**(3), 279–308

DOI: 10.2478/s11772-012-0037-7

History of infrared detectors

A. ROGALSKI*

Institute of Applied Physics, Military University of Technology, 2 Kaliskiego Str., 00–908 Warsaw, Poland

This paper overviews the history of infrared detector materials starting with Herschel's experiment with thermometer on February 11th, 1800. Infrared detectors are in general used to detect, image, and measure patterns of the thermal heat radiation which all objects emit. At the beginning, their development was connected with thermal detectors, such as thermocouples and bolometers, which are still used today and which are generally sensitive to all infrared wavelengths and operate at room temperature. The second kind of detectors, called the photon detectors, was mainly developed during the 20th Century to improve sensitivity and response time. These detectors have been extensively developed since the 1940's. Lead sulphide (PbS) was the first practical IR detector with sensitivity to infrared wavelengths up to ~3 μm. After World War II infrared detector technology development was and continues to be primarily driven by military applications. Discovery of variable band gap HgCdTe ternary alloy by Lawson and co-workers in 1959 opened a new area in IR detector technology and has provided an unprecedented degree of freedom in infrared detector design. Many of these advances were transferred to IR astronomy from Departments of Defence research. Later on civilian applications of infrared technology are frequently called "dual-use technology applications." One should point out the growing utilisation of IR technologies in the civilian sphere based on the use of new materials and technologies, as well as the noticeable price decrease in these high cost technologies. In the last four decades different types of detectors are combined with electronic readouts to make detector focal plane arrays (FPAs). Development in FPA technology has revolutionized infrared imaging. Progress in integrated circuit design and fabrication techniques has resulted in continued rapid growth in the size and performance of these solid state arrays.

Keywords: thermal and photon detectors, lead salt detectors, HgCdTe detectors, microbolometers, focal plane arrays.

Contents

1. Introduction
2. Historical perspective
3. Classification of infrared detectors
   3.1. Photon detectors
   3.2. Thermal detectors
4. Post-War activity
5. HgCdTe era
6. Alternative material systems
   6.1. InSb and InGaAs
   6.2. GaAs/AlGaAs quantum well superlattices
   6.3. InAs/GaInSb strained layer superlattices
   6.4. Hg-based alternatives to HgCdTe
7. New revolution in thermal detectors
8. Focal plane arrays – revolution in imaging systems
   8.1. Cooled FPAs
   8.2. Uncooled FPAs
   8.3. Readiness level of LWIR detector technologies
9. Summary
   References

1. Introduction

Looking back over the past 1000 years we notice that infrared radiation (IR) itself was unknown until 212 years ago when Herschel's experiment with thermometer and prism was first reported. Frederick William Herschel (1738–1822) was born in Hanover, Germany but emigrated to Britain at age 19, where he became well known as both a musician and an astronomer. Herschel became most famous for the discovery of Uranus in 1781 (the first new planet found since antiquity) in addition to two of its major moons, Titania and Oberon. He also discovered two moons of Saturn and infrared radiation. Herschel is also known for the twenty-four symphonies that he composed.

W. Herschel made another milestone discovery – discovery of infrared light on February 11th, 1800. He studied the spectrum of sunlight with a prism [see Fig. 1 in Ref. 1], measuring temperature of each colour. The detector consisted of liquid in a glass thermometer with a specially blackened bulb to absorb radiation. Herschel built a crude monochromator that used a thermometer as a detector, so that he could measure the distribution of energy in sunlight and found that the highest temperature was just beyond the red, what we now call the infrared ('below the red', from the Latin 'infra' – be-

*e-mail: rogan@wat.edu.pl

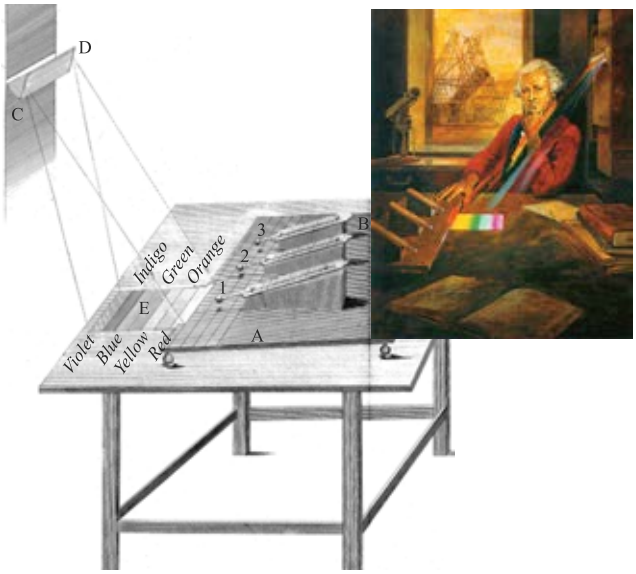

Fig. 1. Herschel's first experiment: A,B – the small stand, 1,2,3 – the thermometers upon it, C,D – the prism at the window, E – the spectrum thrown upon the table, so as to bring the last quarter of an inch of the read colour upon the stand (after Ref. 1). Inside Sir Frederick William Herschel (1738–1822) measures infrared light from the sun – artist's impression (after Ref. 2).

low) – see Fig. 1(b) [2]. In April 1800 he reported it to the Royal Society as dark heat (Ref. 1, pp. 288–290):

Here the thermometer No. 1 rose 7 degrees, in 10 minutes, by an exposure to the full red coloured rays. I drew back the stand, till the centre of the ball of No. 1 was just at the vanishing of the red colour, so that half its ball was within, and half without, the visible rays of the sun... And here the thermometer No. 1 rose, in 16 minutes, $8\frac{3}{4}$ *degrees, when its centre was* $\frac{1}{2}$ *inch out of the visible rays of the sun. Now, as before we had a rising of 9 degrees, and here* $8\frac{3}{4}$ *the difference is almost too trifling to suppose, that this latter situation of the thermometer was much beyond the maximum of the heating power; while, at the same time, the experiment sufficiently indicates, that the place inquired after need not be looked for at a greater distance.*

Making further experiments on what Herschel called the 'calorific rays' that existed beyond the red part of the spectrum, he found that they were reflected, refracted, absorbed and transmitted just like visible light [1,3,4].

The early history of IR was reviewed about 50 years ago in three well-known monographs [5–7]. Many historical information can be also found in four papers published by Barr [3,4,8,9] and in more recently published monograph [10]. Table 1 summarises the historical development of infrared physics and technology [11,12].

2. Historical perspective

For thirty years following Herschel's discovery, very little progress was made beyond establishing that the infrared radiation obeyed the simplest laws of optics. Slow progress in the study of infrared was caused by the lack of sensitive and accurate detectors – the experimenters were handicapped by the ordinary thermometer. However, towards the second decade of the 19th century, Thomas Johann Seebeck began to examine the junction behaviour of electrically conductive materials. In 1821 he discovered that a small electric current will flow in a closed circuit of two dissimilar metallic conductors, when their junctions are kept at different temperatures [13]. During that time, most physicists thought that radiant heat and light were different phenomena, and the discovery of Seebeck indirectly contributed to a revival of the debate on the nature of heat. Due to small output vol- tage of Seebeck's junctions, some μV/K, the measurement of very small temperature differences were prevented. In 1829 L. Nobili made the first thermocouple and improved electrical thermometer based on the thermoelectric effect discovered by Seebeck in 1826. Four years later, M. Melloni introduced the idea of connecting several bismuth-copper thermocouples in series, generating a higher and, therefore, measurable output voltage. It was at least 40 times more sensitive than the best thermometer available and could detect the heat from a person at a distance of 30 ft [8]. The output voltage of such a thermopile structure linearly increases with the number of connected thermocouples. An example of thermopile's prototype invented by Nobili is shown in Fig. 2(a). It consists of twelve large bismuth and antimony elements. The elements were placed upright in a brass ring secured to an adjustable support, and were screened by a wooden disk with a 15-mm central aperture. Incomplete version of the Nobili-Melloni thermopile originally fitted with the brass cone-shaped tubes to collect ra- diant heat is shown in Fig. 2(b). This instrument was much more sensitive than the thermometers previously used and became the most widely used detector of IR radiation for the next half century.

The third member of the trio, Langley's bolometer appeared in 1880 [7]. Samuel Pierpont Langley (1834–1906) used two thin ribbons of platinum foil connected so as to form two arms of a Wheatstone bridge (see Fig. 3) [15]. This instrument enabled him to study solar irradiance far into its infrared region and to measure the intensity of solar radiation at various wavelengths [9,16,17]. The bolometer's sen-

(a) (b)

Fig. 2 . The Nobili-Meloni thermopiles: (a) thermopile's prototype invented by Nobili (ca. 1829), (b) incomplete version of the Nobili--Melloni thermopile (ca. 1831). Museo Galileo – Institute and Museum of the History of Science, Piazza dei Giudici 1, 50122 Florence, Italy (after Ref. 14).

Table 1. Milestones in the development of infrared physics and technology (up-dated after Refs. 11 and 12)

Year	Event
1800	Discovery of the existence of thermal radiation in the invisible beyond the red by W. HERSCHEL
1821	Discovery of the thermoelectric effects using an antimony-copper pair by T.J. SEEBECK
1830	Thermal element for thermal radiation measurement by L. NOBILI
1833	Thermopile consisting of 10 in-line Sb-Bi thermal pairs by L. NOBILI and M. MELLONI
1834	Discovery of the PELTIER effect on a current-fed pair of two different conductors by J.C. PELTIER
1835	Formulation of the hypothesis that light and electromagnetic radiation are of the same nature by A.M. AMPERE
1839	Solar absorption spectrum of the atmosphere and the role of water vapour by M. MELLONI
1840	Discovery of the three atmospheric windows by J. HERSCHEL (son of W. HERSCHEL)
1857	Harmonization of the three thermoelectric effects (SEEBECK, PELTIER, THOMSON) by W. THOMSON (Lord KELVIN)
1859	Relationship between absorption and emission by G. KIRCHHOFF
1864	Theory of electromagnetic radiation by J.C. MAXWELL
1873	Discovery of photoconductive effect in selenium by W. SMITH
1876	Discovery of photovoltaic effect in selenium (photopiles) by W.G. ADAMS and A.E. DAY
1879	Empirical relationship between radiation intensity and temperature of a blackbody by J. STEFAN
1880	Study of absorption characteristics of the atmosphere through a Pt bolometer resistance by S.P. LANGLEY
1883	Study of transmission characteristics of IR-transparent materials by M. MELLONI
1884	Thermodynamic derivation of the STEFAN law by L. BOLTZMANN
1887	Observation of photoelectric effect in the ultraviolet by H. HERTZ
1890	J. ELSTER and H. GEITEL constructed a photoemissive detector consisted of an alkali-metal cathode
1894, 1900	Derivation of the wavelength relation of blackbody radiation by J.W. RAYEIGH and W. WIEN
1900	Discovery of quantum properties of light by M. PLANCK
1903	Temperature measurements of stars and planets using IR radiometry and spectrometry by W.W. COBLENTZ
1905	A. EINSTEIN established the theory of photoelectricity
1911	R. ROSLING made the first television image tube on the principle of cathode ray tubes constructed by F. Braun in 1897
1914	Application of bolometers for the remote exploration of people and aircrafts (a man at 200 m and a plane at 1000 m)
1917	T.W. CASE developed the first infrared photoconductor from substance composed of thallium and sulphur
1923	W. SCHOTTKY established the theory of dry rectifiers
1925	V.K. ZWORYKIN made a television image tube (kinescope) then between 1925 and 1933, the first electronic camera with the aid of converter tube (iconoscope)
1928	Proposal of the idea of the electro-optical converter (including the multistage one) by G. HOLST, J.H. DE BOER, M.C. TEVES, and C.F. VEENEMANS
1929	L.R. KOHLER made a converter tube with a photocathode (Ag/O/Cs) sensitive in the near infrared
1930	IR direction finders based on PbS quantum detectors in the wavelength range 1.5–3.0 μm for military applications (GUDDEN, GÖRLICH and KUTSCHER), increased range in World War II to 30 km for ships and 7 km for tanks (3–5 μm)
1934	First IR image converter
1939	Development of the first IR display unit in the United States (Sniperscope, Snooperscope)
1941	R.S. OHL observed the photovoltaic effect shown by a p-n junction in a silicon
1942	G. EASTMAN (Kodak) offered the first film sensitive to the infrared
1947	Pneumatically acting, high-detectivity radiation detector by M.J.E. GOLAY
1954	First imaging cameras based on thermopiles (exposure time of 20 min per image) and on bolometers (4 min)
1955	Mass production start of IR seeker heads for IR guided rockets in the US (PbS and PbTe detectors, later InSb detectors for Sidewinder rockets)
1957	Discovery of HgCdTe ternary alloy as infrared detector material by W.D. LAWSON, S. NELSON, and A.S. YOUNG
1961	Discovery of extrinsic Ge:Hg and its application (linear array) in the first LWIR FLIR systems
1965	Mass production start of IR cameras for civil applications in Sweden (single-element sensors with optomechanical scanner: AGA Thermografiesystem 660)
1970	Discovery of charge-couple device (CCD) by W.S. BOYLE and G.E. SMITH
1970	Production start of IR sensor arrays (monolithic Si-arrays: R.A. SOREF 1968; IR-CCD: 1970; SCHOTTKY diode arrays: F.D. SHEPHERD and A.C. YANG 1973; IR-CMOS: 1980; SPRITE: T. ELIOTT 1981)
1975	Lunch of national programmes for making spatially high resolution observation systems in the infrared from multielement detectors integrated in a mini cooler (so-called first generation systems): common module (CM) in the United States, thermal imaging common module (TICM) in Great Britain, syteme modulaire termique (SMT) in France
1975	First In bump hybrid infrared focal plane array
1977	Discovery of the broken-gap type-II InAs/GaSb superlattices by G.A. SAI-HALASZ, R. TSU, and L. ESAKI
1980	Development and production of second generation systems [cameras fitted with hybrid HgCdTe(InSb)/Si(readout) FPAs]. First demonstration of two-colour back-to-back SWIR GaInAsP detector by J.C. CAMPBELL, A.G. DENTAI, T.P. LEE, and C.A. BURRUS
1985	Development and mass production of cameras fitted with Schottky diode FPAs (platinum silicide)
1990	Development and production of quantum well infrared photoconductor (QWIP) hybrid second generation systems
1995	Production start of IR cameras with uncooled FPAs (focal plane arrays; microbolometer-based and pyroelectric)
2000	Development and production of third generation infrared systems

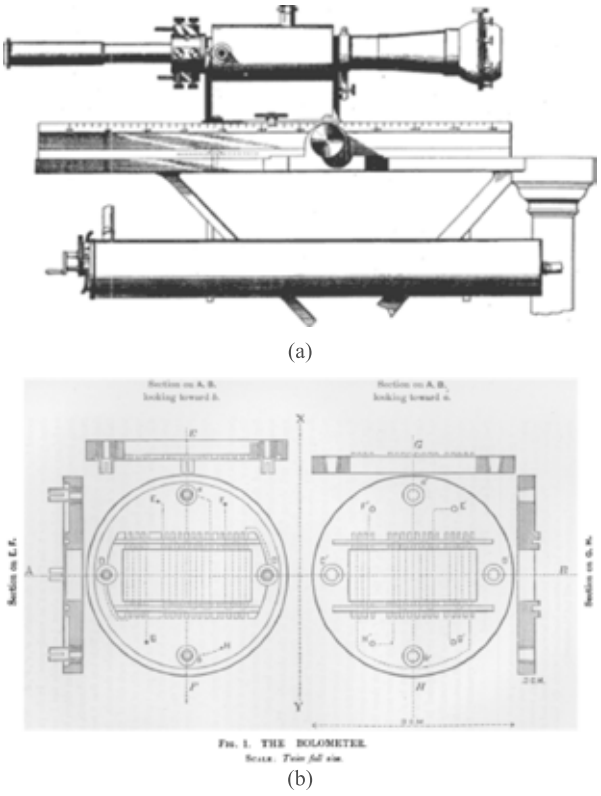

(a)

(b)

Fig. 3. Longley's bolometer (a) composed of two sets of thin platinum strips (b), a Wheatstone bridge, a battery, and a galvanometer measuring electrical current (after Ref. 15 and 16).

sitivity was much greater than that of contemporary thermopiles which were little improved since their use by Melloni. Langley continued to develop his bolometer for the next 20 years (400 times more sensitive than his first efforts). His latest bolometer could detect the heat from a cow at a distance of quarter of mile [9].

From the above information results that at the beginning the development of the IR detectors was connected with thermal detectors. The first photon effect, photoconductive effect, was discovered by Smith in 1873 when he experimented with selenium as an insulator for submarine cables [18]. This discovery provided a fertile field of investigation for several decades, though most of the efforts were of doubtful quality. By 1927, over 1500 articles and 100 patents were listed on photosensitive selenium [19]. It should be mentioned that the literature of the early 1900's shows increasing interest in the application of infrared as solution to numerous problems [7]. A special contribution of William Coblenz (1873–1962) to infrared radiometry and spectroscopy is marked by huge bibliography containing hundreds of scientific publications, talks, and abstracts to his credit [20,21]. In 1915, W. Coblentz at the US National Bureau of Standards develops thermopile detectors, which he uses to measure the infrared radiation from 110 stars. However, the low sensitivity of early infrared instruments prevented the detection of other near-IR sources. Work in infrared astronomy remained at a low level until breakthroughs in the development of new, sensitive infrared detectors were achieved in the late 1950's.

The principle of photoemission was first demonstrated in 1887 when Hertz discovered that negatively charged particles were emitted from a conductor if it was irradiated with ultraviolet [22]. Further studies revealed that this effect could be produced with visible radiation using an alkali metal electrode [23].

Rectifying properties of semiconductor-metal contact were discovered by Ferdinand Braun in 1874 [24], when he probed a naturally-occurring lead sulphide (galena) crystal with the point of a thin metal wire and noted that current flowed freely in one direction only. Next, Jagadis Chandra Bose demonstrated the use of galena-metal point contact to detect millimetre electromagnetic waves. In 1901 he filed a U.S patent for a point-contact semiconductor rectifier for detecting radio signals [25]. This type of contact called cat's whisker detector (sometimes also as crystal detector) played serious role in the initial phase of radio development. However, this contact was not used in a radiation detector for the next several decades. Although crystal rectifiers allowed to fabricate simple radio sets, however, by the mid-1920s the predictable performance of vacuum-tubes replaced them in most radio applications.

The period between World Wars I and II is marked by the development of photon detectors and image converters and by emergence of infrared spectroscopy as one of the key analytical techniques available to chemists. The image converter, developed on the eve of World War II, was of tremendous interest to the military because it enabled man to see in the dark.

The first IR photoconductor was developed by Theodore W. Case in 1917 [26]. He discovered that a substance composed of thallium and sulphur (Tl_2S) exhibited photoconductivity. Supported by the US Army between 1917 and 1918, Case adapted these relatively unreliable detectors for use as sensors in an infrared signalling device [27]. The prototype signalling system, consisting of a 60-inch diameter searchlight as the source of radiation and a thallous sulphide detector at the focus of a 24-inch diameter paraboloid mirror, sent messages 18 miles through what was described as 'smoky atmosphere' in 1917. However, instability of resistance in the presence of light or polarizing voltage, loss of responsivity due to over-exposure to light, high noise, sluggish response and lack of reproducibility seemed to be inherent weaknesses. Work was discontinued in 1918; communication by the detection of infrared radiation appeared distinctly unpromising. Later Case found that the addition of oxygen greatly enhanced the response [28].

The idea of the electro-optical converter, including the multistage one, was proposed by Holst *et al*. in 1928 [29]. The first attempt to make the converter was not successful. A working tube consisted of a photocathode in close proximity to a fluorescent screen was made by the authors in 1934 in Philips firm.

In about 1930, the appearance of the Cs-O-Ag phototube, with stable characteristics, to great extent discouraged further development of photoconductive cells until about 1940. The Cs-O-Ag photocathode (also called S-1) elabo-

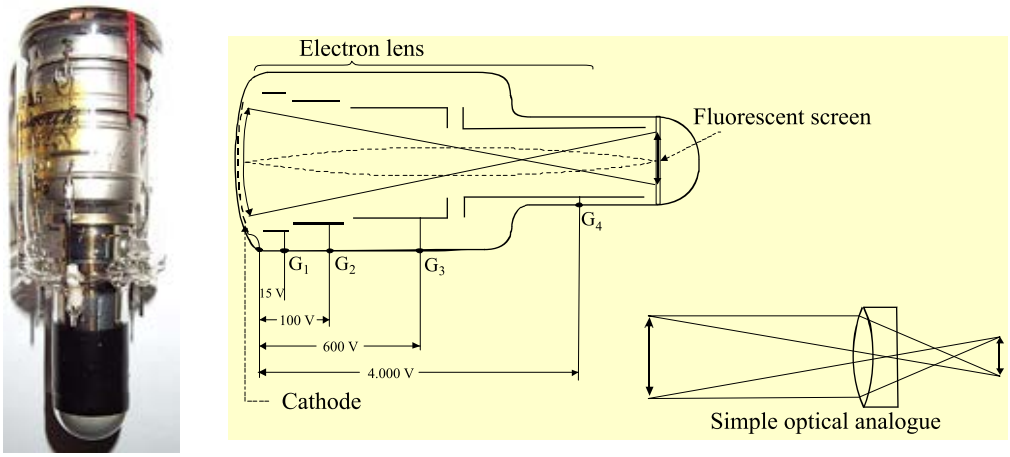

(a) (b)

Fig. 4. The original 1P25 image converter tube developed by the RCA (a). This device measures 115×38 mm overall and has 7 pins. It operation is indicated by the schematic drawing (b).

rated by Koller and Campbell [30] had a quantum efficiency two orders of magnitude above anything previously studied, and consequently a new era in photoemissive devices was inaugurated [31]. In the same year, the Japanese scientists S. Asao and M. Suzuki reported a method for enhancing the sensitivity of silver in the S-1 photocathode [32]. Consisted of a layer of caesium on oxidized silver, S-1 is sensitive with useful response in the near infrared, out to approximately 1.2 μm, and the visible and ultraviolet region, down to 0.3 μm. Probably the most significant IR development in the United States during 1930's was the Radio Corporation of America (RCA) IR image tube. During World War II, near-IR (NIR) cathodes were coupled to visible phosphors to provide a NIR image converter. With the establishment of the National Defence Research Committee, the development of this tube was accelerated. In 1942, the tube went into production as the RCA 1P25 image converter (see Fig. 4). This was one of the tubes used during World War II as a part of the "Snooperscope" and "Sniperscope," which were used for night observation with infrared sources of illumination. Since then various photocathodes have been developed including bialkali photocathodes for the visible region, multialkali photocathodes with high sensitivity extending to the infrared region and alkali halide photocathodes intended for ultraviolet detection.

The early concepts of image intensification were not basically different from those today. However, the early devices suffered from two major deficiencies: poor photocathodes and poor coupling. Later development of both cathode and coupling technologies changed the image intensifier into much more useful device. The concept of image intensification by cascading stages was suggested independently by number of workers. In Great Britain, the work was directed toward proximity focused tubes, while in the United State and in Germany – to electrostatically focused tubes. A history of night vision imaging devices is given by Biberman and Sendall in monograph *Electro-Optical Imaging: System Performance and Modelling*, SPIE Press, 2000 [10]. The Biberman's monograph describes the basic trends of infrared optoelectronics development in the USA, Great Britain, France, and Germany. Seven years later Ponomarenko and Filachev completed this monograph writing the book *Infrared Techniques and Electro-Optics in Russia: A History 1946-2006*, SPIE Press, about achievements of IR techniques and electrooptics in the former USSR and Russia [33].

In the early 1930's, interest in improved detectors began in Germany [27,34,35]. In 1933, Edgar W. Kutzscher at the University of Berlin, discovered that lead sulphide (from natural galena found in Sardinia) was photoconductive and had response to about 3 μm. B. Gudden at the University of Prague used evaporation techniques to develop sensitive PbS films. Work directed by Kutzscher, initially at the University of Berlin and later at the Electroacustic Company in Kiel, dealt primarily with the chemical deposition approach to film formation. This work ultimately lead to the fabrication of the most sensitive German detectors. These works were, of course, done under great secrecy and the results were not generally known until after 1945. Lead sulphide photoconductors were brought to the manufacturing stage of development in Germany in about 1943. Lead sulphide was the first practical infrared detector deployed in a variety of applications during the war. The most notable was the Kiel IV, an airborne IR system that had excellent range and which was produced at Carl Zeiss in Jena under the direction of Werner K. Weihe [6].

In 1941, Robert J. Cashman improved the technology of thallous sulphide detectors, which led to successful production [36,37]. Cashman, after success with thallous sulphide detectors, concentrated his efforts on lead sulphide detectors, which were first produced in the United States at Northwestern University in 1944. After World War II Cashman found that other semiconductors of the lead salt family (PbSe and PbTe) showed promise as infrared detectors [38]. The early detector cells manufactured by Cashman are shown in Fig. 5.

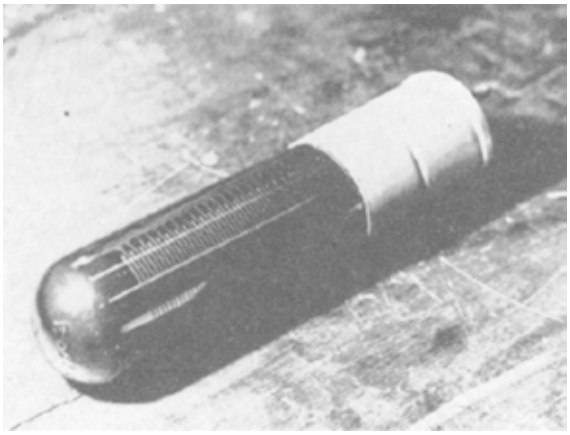

(a)

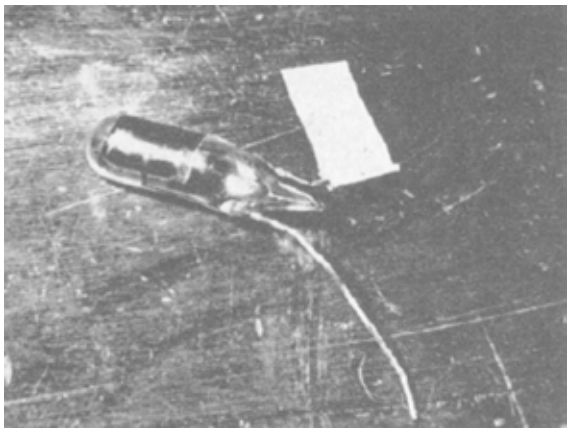

(b)

Fig. 5. Cashman's detector cells: (a) Tl_2S cell (ca. 1943): a grid of two intermeshing comb-line sets of conducting paths were first provided and next the T_2S was evaporated over the grid structure; (b) PbS cell (ca. 1945) the PbS layer was evaporated on the wall of the tube on which electrical leads had been drawn with aquadag (after Ref. 38).

After 1945, the wide-ranging German trajectory of research was essentially the direction continued in the USA, Great Britain and Soviet Union under military sponsorship after the war [27,39]. Kutzscher's facilities were captured by the Russians, thus providing the basis for early Soviet detector development. From 1946, detector technology was rapidly disseminated to firms such as Mullard Ltd. in Southampton, UK, as part of war reparations, and sometimes was accompanied by the valuable tacit knowledge of technical experts. E.W. Kutzscher, for example, was flown to Britain from Kiel after the war, and subsequently had an important influence on American developments when he joined Lockheed Aircraft Co. in Burbank, California as a research scientist.

Although the fabrication methods developed for lead salt photoconductors was usually not completely understood, their properties are well established and reproducibility could only be achieved after following well-tried recipes. Unlike most other semiconductor IR detectors, lead salt photoconductive materials are used in the form of polycrystalline films approximately 1 μm thick and with individual crystallites ranging in size from approximately 0.1–1.0 μm. They are usually prepared by chemical deposition using empirical recipes, which generally yields better uniformity of response and more stable results than the evaporative methods. In order to obtain high-performance detectors, lead chalcogenide films need to be sensitized by oxidation. The oxidation may be carried out by using additives in the deposition bath, by post-deposition heat treatment in the presence of oxygen, or by chemical oxidation of the film. The effect of the oxidant is to introduce sensitizing centres and additional states into the bandgap and thereby increase the lifetime of the photoexcited holes in the p-type material.

3. Classification of infrared detectors

Observing a history of the development of the IR detector technology after World War II, many materials have been investigated. A simple theorem, after Norton [40], can be stated: "All physical phenomena in the range of about 0.1–1 eV will be proposed for IR detectors". Among these effects are: thermoelectric power (thermocouples), change in electrical conductivity (bolometers), gas expansion (Golay cell), pyroelectricity (pyroelectric detectors), photon drag, Josephson effect (Josephson junctions, SQUIDs), internal emission (PtSi Schottky barriers), fundamental absorption (intrinsic photodetectors), impurity absorption (extrinsic photodetectors), low dimensional solids [superlattice (SL), quantum well (QW) and quantum dot (QD) detectors], different type of phase transitions, etc.

Figure 6 gives approximate dates of significant development efforts for the materials mentioned. The years during World War II saw the origins of modern IR detector technology. Recent success in applying infrared technology to remote sensing problems has been made possible by the successful development of high-performance infrared detectors over the last six decades. Photon IR technology combined with semiconductor material science, photolithography technology developed for integrated circuits, and the impetus of Cold War military preparedness have propelled extraordinary advances in IR capabilities within a short time period during the last century [41].

The majority of optical detectors can be classified in two broad categories: photon detectors (also called quantum detectors) and thermal detectors.

3.1. Photon detectors

In photon detectors the radiation is absorbed within the material by interaction with electrons either bound to lattice atoms or to impurity atoms or with free electrons. The observed electrical output signal results from the changed electronic energy distribution. The photon detectors show a selective wavelength dependence of response per unit incident radiation power (see Fig. 8). They exhibit both a good signal-to-noise performance and a very fast response. But to achieve this, the photon IR detectors require cryogenic cooling. This is necessary to prevent the thermal

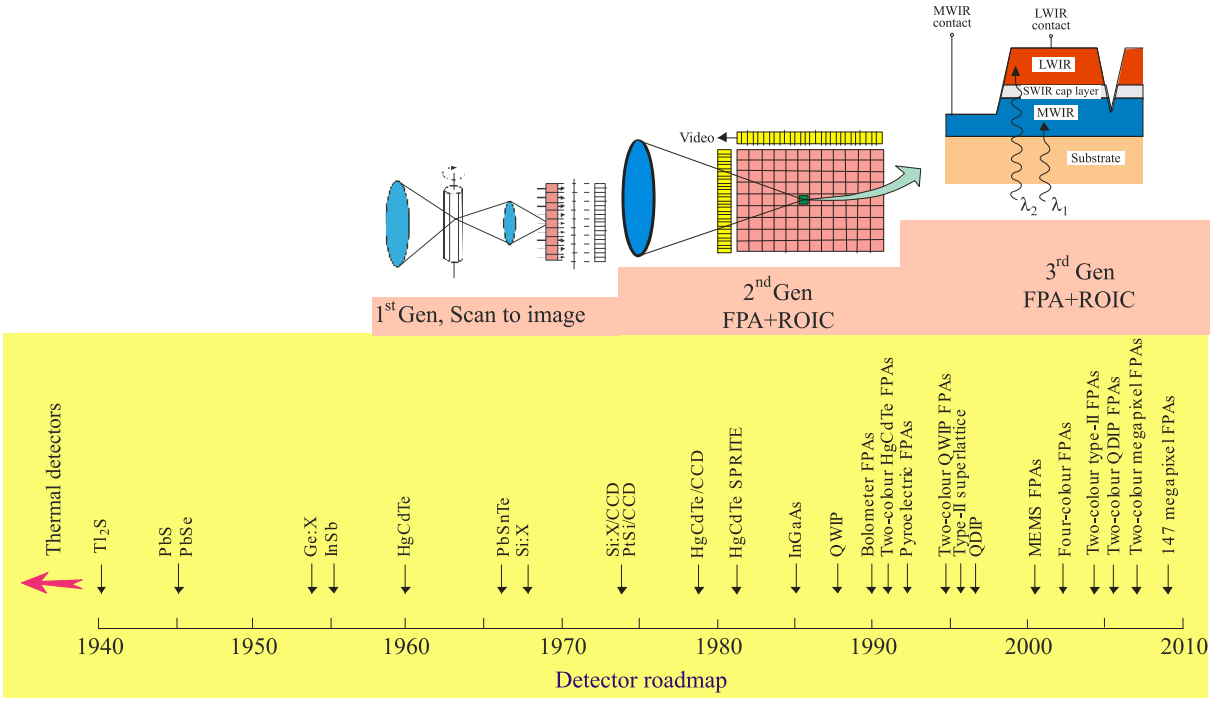

Fig. 6. History of the development of infrared detectors and systems. Three generation systems can be considered for principal military and civilian applications: 1st Gen (scanning systems), 2nd Gen (staring systems – electronically scanned) and 3rd Gen (multicolour functionality and other on-chip functions).

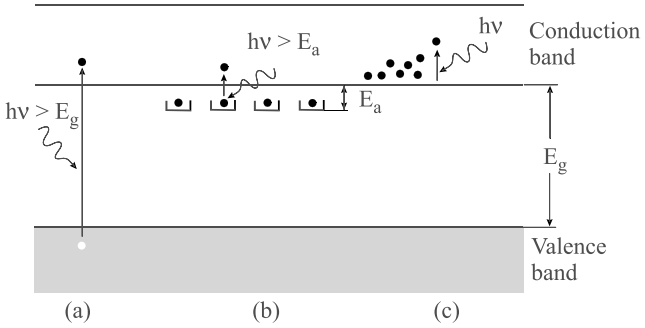

Fig. 7. Fundamental optical excitation processes in semiconductors: (a) intrinsic absorption, (b) extrinsic absorption, (c) free carrier absorption.

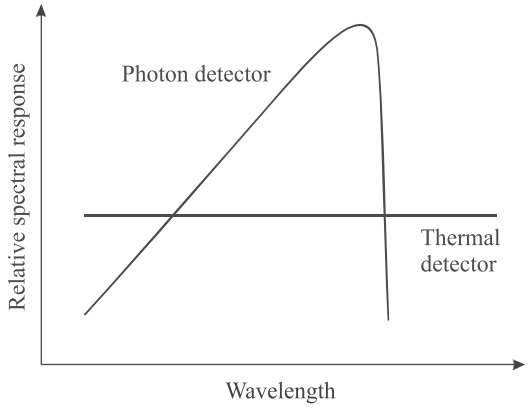

Fig. 8. Relative spectral response for a photon and thermal detector.

generation of charge carriers. The thermal transitions compete with the optical ones, making non-cooled devices very noisy.

The spectral current responsivity of photon detectors is equal to

$$R_i = \frac{\lambda \eta}{hc} qg\,, \tag{1}$$

where λ is the wavelength, h is the Planck's constant, c is the velocity of light, q is the electron charge, and g is the photoelectric current gain. The current that flows through the contacts of the device is noisy due to the statistical nature of the generation and recombination processes – fluctuation of optical generation, thermal generation, and radiative and nonradiative recombination rates. Assuming that the current gain for the photocurrent and the noise current are the same, the noise current is

$$I_n^2 = 2q^2 g^2 (G_{op} + G_{th} + R)\Delta f, \tag{2}$$

where G_{op} is the optical generation rate, G_{th} is the thermal generation rate, R is the resulting recombination rate, and Δf is the frequency band.

It was found by Jones [42], that for many detectors the noise equivalent power (*NEP*) is proportional to the square root of the detector signal that is proportional to the detector area, A_d. The normalized detectivity D^* (or *D*-star) suggested by Jones is defined as

$$D^* = \frac{(A_d)^{1/2}}{NEP}. \tag{3}$$

Detectivity, D^*, is the main parameter to characterize normalized signal-to-noise performance of detectors and can be also defined as

$$D^* = \frac{R_i (A_d \Delta f)^{1/2}}{I_n}. \tag{4}$$

The importance of D^* is that this figure of merit permits comparison of detectors of the same type, but having different areas. Either a spectral or blackbody D^* can be defined in terms of corresponding type of *NEP*.

At equilibrium, the generation and recombination rates are equal. In this case

$$D^* = \frac{\lambda \eta}{2hc(Gt)^{1/2}}. \tag{5}$$

Background radiation frequently is the main source of noise in a IR detector. Assuming no contribution due to recombination,

$$I_n^2 = 2\Phi_B A_d \eta q^2 g^2 \Delta f, \tag{6}$$

where Φ_B is the background photon flux density. Therefore, at the background limited performance conditions (BLIP performance)

$$D^*_{BLIP} = \frac{\lambda}{hc}\left(\frac{\eta}{\Phi_B}\right)^{1/2}. \tag{7}$$

Once background-limited performance is reached, quantum efficiency, η, is the only detector parameter that can influence a detector's performance.

Depending on the nature of the interaction, the class of photon detectors is further sub-divided into different types. The most important are: intrinsic detectors, extrinsic detectors, photoemissive (Schottky barriers). Different types of detectors are described in details in monograph *Infrared Detectors* [41]. Figure 9 shows spectral detectivity curves for a number of commercially available IR detectors.

3.2. Thermal detectors

The second class of detectors is composed of thermal detectors. In a thermal detector shown schematically in Fig. 10, the incident radiation is absorbed to change the material temperature and the resultant change in some physical property is used to generate an electrical output. The detector is suspended on legs which are connected to the heat sink. The signal does not depend upon the photonic nature of the incident radiation. Thus, thermal effects are generally wavelength independent (see Fig. 8); the signal depends upon the

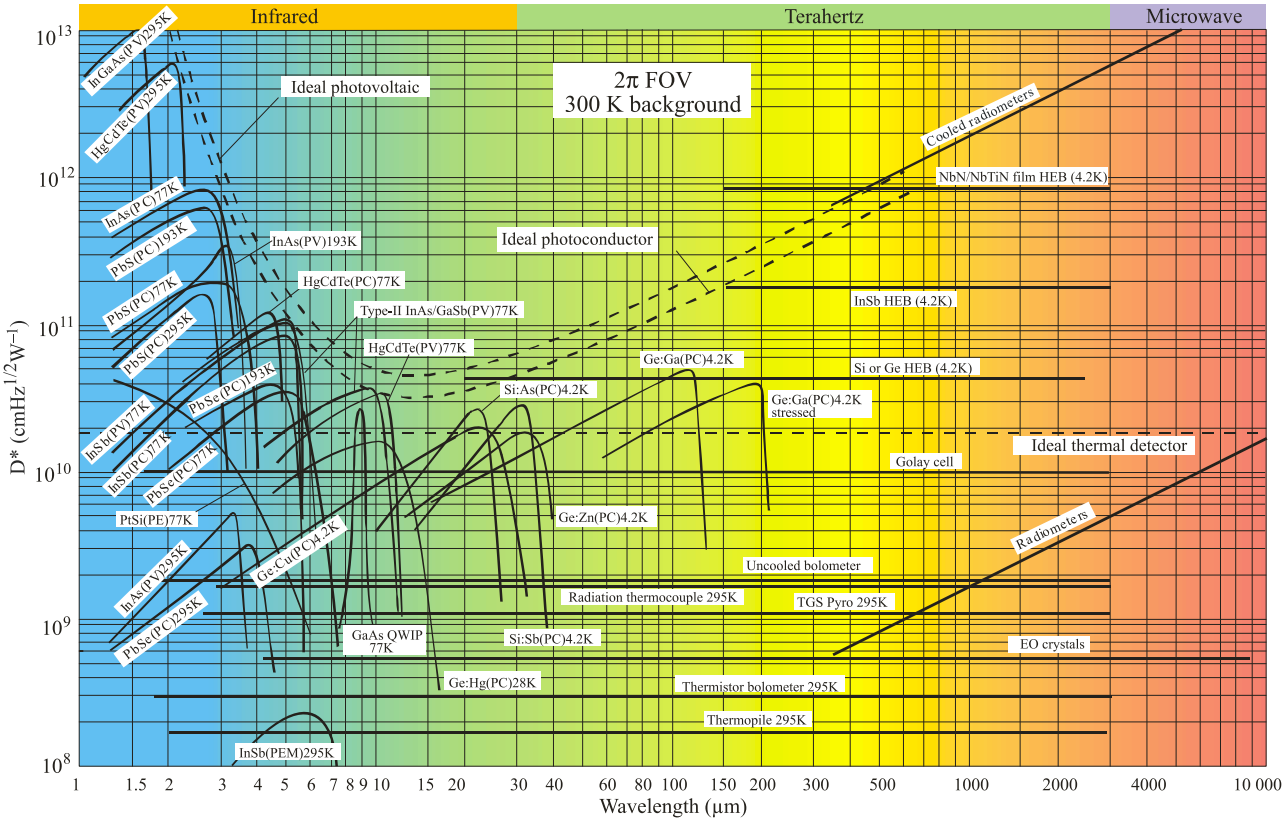

Fig. 9. Comparison of the D^* of various available detectors when operated at the indicated temperature. Chopping frequency is 1000 Hz for all detectors except the thermopile (10 Hz), thermocouple (10 Hz), thermistor bolometer (10 Hz), Golay cell (10 Hz) and pyroelectric detector (10 Hz). Each detector is assumed to view a hemispherical surrounding at a temperature of 300 K. Theoretical curves for the background-limited D^* (dashed lines) for ideal photovoltaic and photoconductive detectors and thermal detectors are also shown. PC – photoconductive detector, PV – photovoltaic detector, PEM – photoelectromagnetic detector, and HEB – hot electron bolometer.

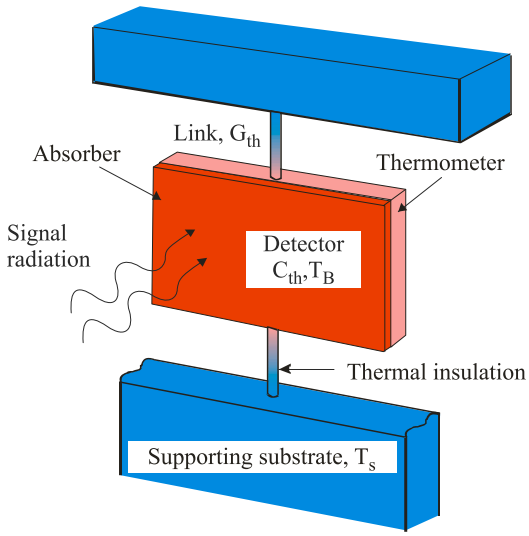

Fig. 10. Schematic diagram of thermal detector.

radiant power (or its rate of change) but not upon its spectral content. Since the radiation can be absorbed in a black surface coating, the spectral response can be very broad. Attention is directed toward three approaches which have found the greatest utility in infrared technology, namely, bolometers, pyroelectric and thermoelectric effects. The thermopile is one of the oldest IR detectors, and is a collection of thermocouples connected in series in order to achieve better temperature sensitivity. In pyroelectric detectors a change in the internal electrical polarization is measured, whereas in the case of thermistor bolometers a change in the electrical resistance is measured. For a long time, thermal detectors were slow, insensitive, bulky and costly devices. But with developments of the semiconductor technology, they can be optimized for specific applications. Recently, thanks to conventional CMOS processes and development of MEMS, the detector's on-chip circuitry technology has opened the door to a mass production.

Usually, a bolometer is a thin, blackened flake or slab, whose impedance is highly temperature dependent. Bolometers may be divided into several types. The most commonly used are metal, thermistor and semiconductor bolometers. A fourth type is the superconducting bolometer. This bolometer operates on a conductivity transition in which the resistance changes dramatically over the transition temperature range. Figure 11 shows schematically the temperature dependence of resistance of different types of bolometers.

Many types of thermal detectors are operated in wide spectral range of electromagnetic radiation. The operation principles of thermal detectors are described in many books; see e.g., Refs. 5, 6, 41, and 43.

4. Post-War activity

It was inevitable that the military would recognize the potential of night vision. However, the military IR technology was in its infancy at the end of World War II. The IR hardware activities

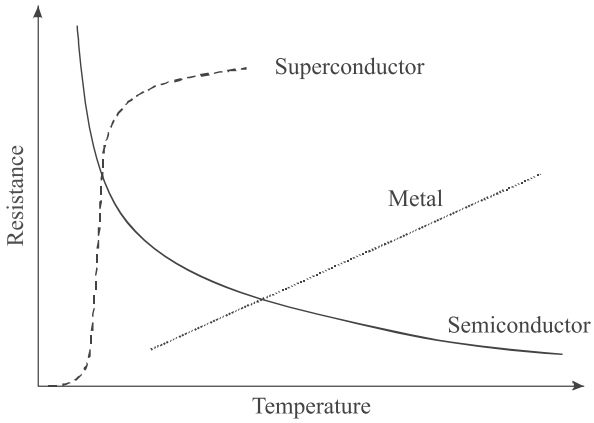

Fig. 11. Temperature dependence of resistance of three bolometer material types.

at the beginning of 1950s of the last century involved mainly simple radiometric instruments (see Fig. 12) and passive night vision technology (see Fig. 13) capable of allowing vision under ambient starlight conditions.

Immediately after the war, communications, fire control and search systems began to stimulate a strong development effort of lead salt detector technology that has extended to the present day. The IR systems were built by using single-element-cooled lead salt detectors, primarily for anti--air-missile seekers. The Sidewinder heat-seeking infrared--guided missiles received a great deal of public attention [46]. The missile entered service with the United States

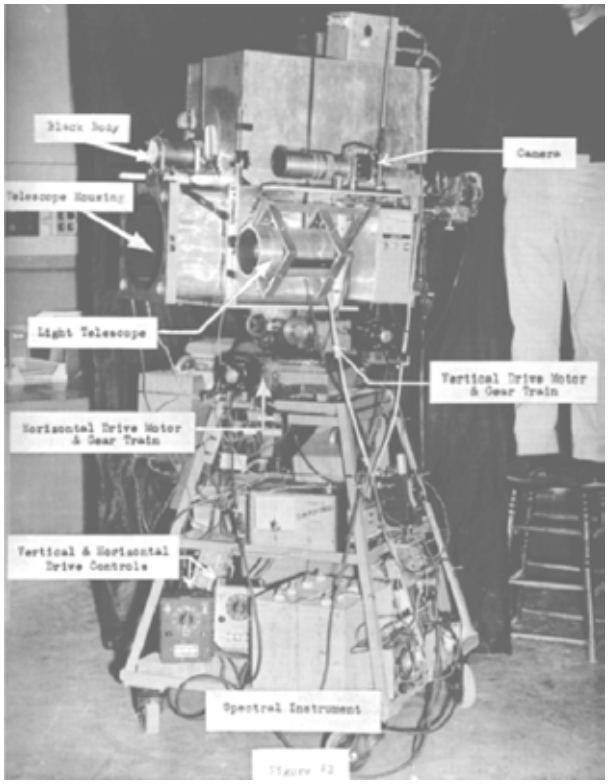

Fig. 12. Spectral radiometer used for early measurements of infrared terrain signatures using a PbTe detector (after Ref. 44).

Fig. 13. TVS-4 Night Observation Device – 1st generation intensifier used only at the night sky illumination. It had an 8 "aperture and was 30" long (after Ref. 45).

Navy in the mid-1950s and variants and upgrades remain in active service with many air forces after six decades. Early Sidewinder models (see Fig. 13 [47]) used uncooled lead sulphide photoconductive detector. From the AIM-9D Sidewinder on, the PbS detector was cooled, which reduced the self generated noise in the detector material. First generation imagers utilized scanned single-element detectors and linear arrays. In the MWIR region (3–5 μm) apart from PbSe, early systems employed InSb.

After 60 years, low-cost versatile PbS and PbSe polycrystalline thin films remain the photoconductive detectors of choice for many applications in the 1–3 μm and 3–5 μm spectral range. Current development with lead salts is in the focal plane arrays (FPAs) configuration.

The first extrinsic photoconductive detectors were reported in the early 1950s [48–50] after the discovery of the transistor, which stimulated a considerable improvement in the growth and material purification techniques. Since the

Fig. 14. Prototype Sidewinder-1 missile on an AD-4 Skyraider during flight testing (after Ref. 47).

techniques for controlled impurity introduction became available for germanium at an earlier date, the first high performance extrinsic detectors were based on germanium. Extrinsic photoconductive response from copper, mercury, zinc and gold impurity levels in germanium gave rise to devices using in the 8- to 14-μm long wavelength IR (LWIR) spectral window and beyond the 14- to 30-μm very long wavelength IR (VLWIR) region. The extrinsic photoconductors were widely used at wavelengths beyond 10 μm prior to the development of the intrinsic detectors. They must be operated at lower temperatures to achieve performance similar to that of intrinsic detectors and sacrifice in quantum efficiency is required to avoid thick detectors.

The discovery in the early 1960s of extrinsic Hg-doped germanium [51] led to the first forward looking infrared (FLIR) systems operating in the LWIR spectral window using linear arrays. Ge:Hg with a 0.09-eV activation energy was a good match to the LWIR spectral window, however, since the detection mechanism was based on an extrinsic excitation, it required a two-stage cooler to operate at 25 K. The first real production FLIR program based upon Ge:Hg was built for the Air Force B52 Aircraft in 1969 [10]. It used a 176-element array of Ge:Hg elements and provided excellent imaging, however, the two-stage cooler had limited lifetime and high system maintenance.

In 1967 the first comprehensive extrinsic Si detector-oriented paper was published by Soref [52]. However, the state of extrinsic Si was not changed significantly. Although Si has several advantages over Ge (namely, a lower dielectric constant giving shorter dielectric relaxation time and lower capacitance, higher dopant solubility and larger photoionization cross section for higher quantum efficiency, and lower refractive index for lower reflectance), these were not sufficient to warrant the necessary development efforts needed to bring it to the level of the, by then, highly developed Ge detectors. After being dormant for about ten years, extrinsic Si was reconsidered after the invention of charge-coupled devices (CCDs) by Boyle and Smith [53]. In 1973, Shepherd and Yang [54] proposed the metal-silicide/silicon Schottky-barrier detectors. For the first time it became possible to have much more sophisticated readout schemes – both detection and readout could be implemented in one common silicon chip.

Beginning in the 1950's, rapid advances were being made in narrow bandgap semiconductors that would later prove useful in extending wavelength capabilities and improving sensitivity. The first such material was InSb, a member of the newly discovered III-V compound semiconductor family. The interest in InSb stemmed not only from its small energy gap, but also from the fact that it could be prepared in single crystal form using a conventional technique. The end of the 1950s and the beginning of the 1960s saw the introduction of narrow gap semiconductor alloys in III-V ($InAs_{1-x}Sb_x$), IV-VI ($Pb_{1-x}Sn_xTe$), and II-VI ($Hg_{1-x}Cd_xTe$) material systems. These alloys allowed the bandgap of the semiconductor and hence the spectral response of the detector to be custom tailored for specific applications. In 1959,

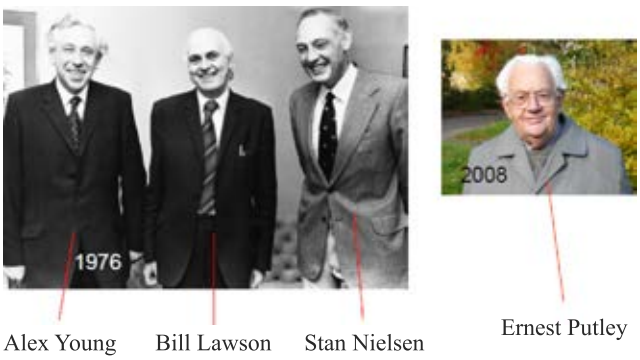

Fig. 15. The discoverers of HgCdTe ternary alloy (after Ref. 56).

research by Lawson and co-workers [55] triggered development of variable bandgap $Hg_{1-x}Cd_xTe$ (HgCdTe) alloys. Figure 15 shows the three Royal Radar Establishment inventors of HgCdTe (W.D. Lawson, S. Nielson, and A.S. Young) that disclosed the compound ternary alloy in a 1957 patent [56]. They were joined by E.H. Putley in the first publication [55].

The Lawson's *et al*. first paper reported both photoconductive and photovoltaic HgCdTe response at the wavelength extending out to 12 μm. Soon thereafter, working under a U.S. Air Force contract with the objective of devising an 8–12-μm background-limited semiconductor IR detector that would operate at temperatures as high as 77 K, the group lead by Kruse at the Honeywell Corporate Research Centre in Hopkins, Minnesota, developed a modified Bridgman crystal growth technique for HgCdTe. They soon reported both photoconductive and photovoltaic detection in rudimentary HgCdTe devices [57]. The parallel programs were carried out at Texas Instruments and SBRC.

The fundamental properties of narrow-gap semiconductors (high optical absorption coefficient, high electron mobility and low thermal generation rate), together with the capability for bandgap engineering, make these alloy systems almost ideal for a wide range of IR detectors. The difficulties in growing HgCdTe material, significantly due to the high vapour pressure of Hg, encouraged the development of alternative detector technologies over the past forty years. One of these was PbSnTe, which was vigorously pursued in parallel with HgCdTe in the late 60s, and early 70s [58,59]. PbSnTe was comparatively easy to grow and good quality LWIR photodiodes and lasers were readily demonstrated.

Figure 16 shows the liquidus and solidus lines in three pseudobinary systems. In comparison with PbTe-SnTe, the wide separation between the HgCdTe liquidus and solidus leads to marked segregation between CdTe and HgTe, what is instrumental in the development of the bulk growth techniques to this system. In addition to solidus-liquidus separation, high-Hg partial pressure are also influential both during growth and post-growth heat treatments.

In the review paper published in 1974 [59], Harman and Melngailis, both involved in studies of HgCdTe and PbSnTe ternary alloys in Massachusetts Institute of Technology, wrote:

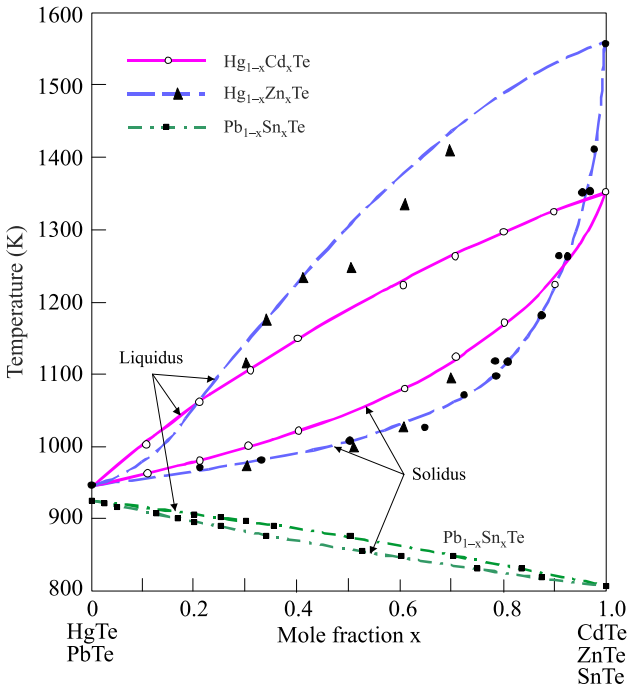

Fig. 16. Liquidus and solidus lines in the HgTe-CdTe, HgTe-ZnTe and PbTe-SnTe pseudobinary systems.

> *In comparing the two materials we anticipate that $Pb_{1-x}Sn_xTe$ will be more widely used in the future for detection of blackbody radiation in the 8–14-μm region because crystal growth techniques for this alloy are potentially cheaper and adaptable to mass production. In addition, $Pb_{1-x}Sn_xTe$ appears to be more stable and less likely to degrade at elevated temperatures than $Hg_{1-x}Cd_xTe$. However, for heterodyne detection and other high-speed applications, $Hg_{1-x}Cd_xTe$ can be expected to be more useful at frequencies in the GHz range because of the inherent advantage of a lower dielectric constant.*

Several years later, this opinion was completely changed. In the late 1970s the development of IV-VI alloy photodiodes was discontinued because the chalcogenides suffered two significant drawbacks. The first was a high dielectric constant that resulted in high diode capacitance and therefore limited frequency response (for PbSnTe the observed values of the static dielectric constant have been widely distributed from 400 to 5800, and at the same temperature these values have been scattered in the range up to one order of magnitude [60]). For scanning systems under development at that time, this was a serious limitation. However, for staring imaging systems under development today using 2D arrays, this would not be as significant of an issue.

The second drawback to IV-VI compounds is their very high thermal coefficients of expansion (TEC) [61]. This limited their applicability in hybrid configurations with silicon multiplexers. Differences in TEC between the readout and detector structure can lead to failure of the indium bonds after repeated thermal cycling from room temperature

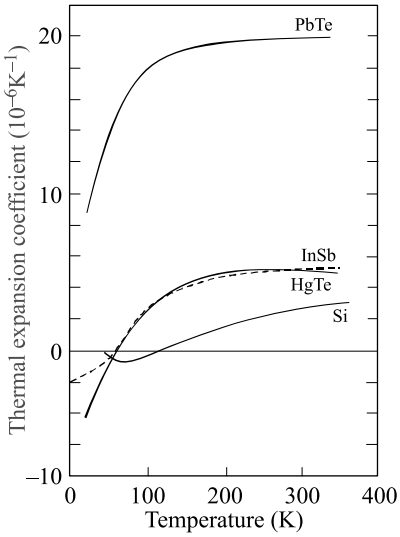

Fig. 17. Linear TEC of PbTe, InSb, HgTe and Si versus temperature (after Ref. 61).

to the cryogenic temperature of operation [62]. Figure 17 shows dependence of the thermal expansion coefficient of PbTe, InSb, HgTe and Si on temperature. At room temperature, the TCE HgTe and CdTe is about 5×10^{-6} K^{-1}, while that of PbSnTe is in the range of 20×10^{-6} K^{-1}. This results in much greater TCE mismatch with silicon (TCE about 3×10^{-6} K^{-1}).

The material technology development was and continues to be primarily for military applications. In the United State, Vietnam War caused the military services to initiate the development of IR systems that could provide imagery arising from the thermal emission of terrain, vehicles, buildings and people. As photolithography became available in the early 1960s, it was applied to make infrared detector arrays. Linear array technology was first applied to PbS, PbSe, and InSb detectors. The first LWIR FLIR system was built in 1969 by using Ge:Hg linear arrays. In that time it was clear from theory that intrinsic HgCdTe detector (where the optical transitions were direct transitions between the valence band and the conduction band) could achieve the same sensitivity at much higher operating temperature. Typically, to obtain the background-limited performance (BLIP), detectors for the 3–5-μm spectral region can operate at 200 K or less, while those for the 8–14-μm – at liquid nitrogen temperature. Early recognition of the significance of this fact led to intensive development of HgCdTe detectors in a number of countries including England, France, Germany, Poland, the former Soviet Union and the United States [63]. However, a little has been written about the early development years; e.g. the existence of work going on in the United States was classified until the late 1960s. More details can be found in papers of *Proceedings of SPIE*, Vol. 7298, with the 35th conference in Infrared Technology and Applications held in Orlando, Florida, April 13–17, 2009, where a special session was organized to celebrate the 50th anniversary of HgCdTe discovery.

5. HgCdTe era

Discovery of variable band gap HgCdTe alloy by Lawson and co-workers in 1959 [55] has provided an unprecedented degree of freedom in infrared detector design. The bandgap energy tunability results in IR detector applications that span the short wavelength IR (SWIR: 1–3 μm), middle wavelength (MWIR: 3–5 μm), long wavelength (LWIR: 8–14 μm), and very long wavelength (VLWIR: 14–30 μm) ranges. HgCdTe technology development was and continues to be primarily for military applications.

A negative aspect of support by defence agencies has been the associated secrecy requirements that inhibit meaningful collaborations among research teams on a national and especially on an international level. In addition, the primary focus has been on focal plane array (FPA) demonstration and much less on establishing the knowledge base. Nevertheless, significant progress has been made over four decades. At present, HgCdTe is the most widely used variable gap semiconductor for IR photodetectors. Over the years it has successfully fought off major challenges from extrinsic silicon and lead-tin telluride devices, but despite that it has more competitors today than ever before. These include Schottky barriers on silicon, SiGe heterojunctions, AlGaAs multiple quantum wells, GaInSb strain layer superlattices, high temperature superconductors and especially two types of thermal detectors: pyroelectric detectors and silicon bolometers. It is interesting, however, that none of these competitors can compete in terms of fundamental properties. They may promise to be more manufacturable, but never to provide higher performance or, with the exception of thermal detectors, to operate at higher or even comparable temperatures. It should be noticed however, that from physics point of view, the type II GaInSb superlattice is an extremely attractive proposition.

Figure 18 gives approximate dates of significant development efforts for HgCdTe IR detectors; instead Fig. 19 gives additional insight in time line of the evolution of detectors and key developments in process technology [64].

Photoconductive devices had been built in the US as early as 1964 at Texas Instruments after development of the modified Bridgman crystal growth technique. The first report of a junction intentionally formed to make an HgCdTe

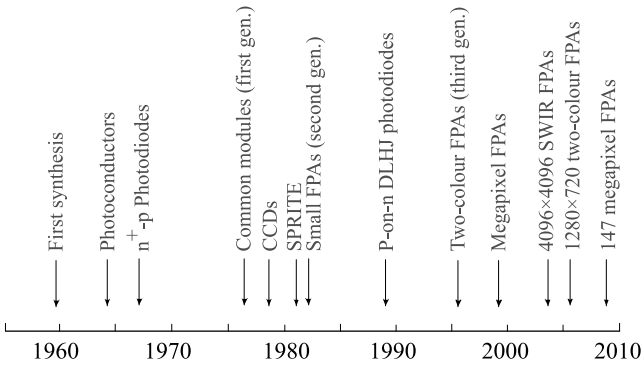

Fig. 18. History of the development of HgCdTe detectors.

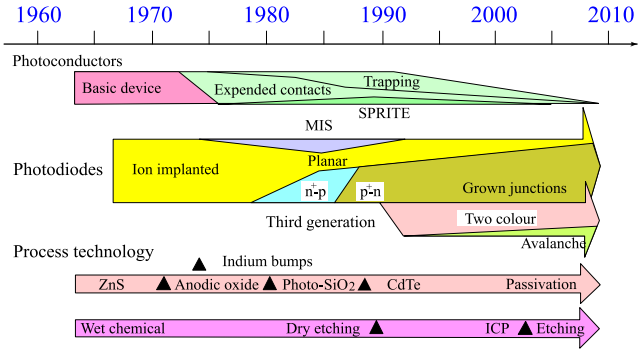

Fig. 19. A time line of the evolution of HgCdTe IR detectors and key developments in process technology which made them possible (after Ref. 64).

photodiode was by Verie and Granger [65], who used Hg in-diffusion into p-type material doped with Hg vacancies. The first important application of HgCdTe photodiodes was as high-speed detectors for CO_2 laser radiation [66]. The French pavilion at the 1967 Montreal Expo illustrated a CO_2 laser system with HgCdTe photodiode. However, the high performance medium wavelength IR (MWIR) and LWIR linear arrays developed and manufactured in the 1970s were n-type photoconductors used in the first generation scanning systems. In 1969 Bartlett *et al*. [67] reported background limited performance of photoconductors operated at 77 K in the LWIR spectral region. The advantage in material preparation and detector technology have led to devices approaching theoretical limits of responsivity and detectivity over wide ranges of temperature and background [68].

HgCdTe has inspired the development of the three "generations" of detector devices (see Fig. 6). In the late 1960s and early 1970s, first-generation linear arrays [in which an electrical contact for each element of a multielement array is brought off the cryogenically-cooled focal plane to the outside, where there is one electronic channel at ambient temperature for each detector element – see Fig. 20(a)] of intrinsic photoconductive PbS, PbSe, HgCdTe detectors were developed. The first generation scanning system does not include multiplexing functions in the focal plane. These allowed LWIR FLIR systems to operate with a single-stage cryoengine, making the systems much more compact, lighter, and requiring significantly less power consumption. The simplest scanning linear FPA consists of a row of detectors. An image is generated by scanning the scene across the strip using, as a rule, a mechanical scanner. At standard video frame rates, at each pixel (detector) a short integration time has been applied and the total charges are accommodated. The US common module HgCdTe arrays employ 60, 120 or 180 photoconductive elements depending on the application. An example of 180-element common module FPA mounted on a dewar stem is shown in Fig. 21.

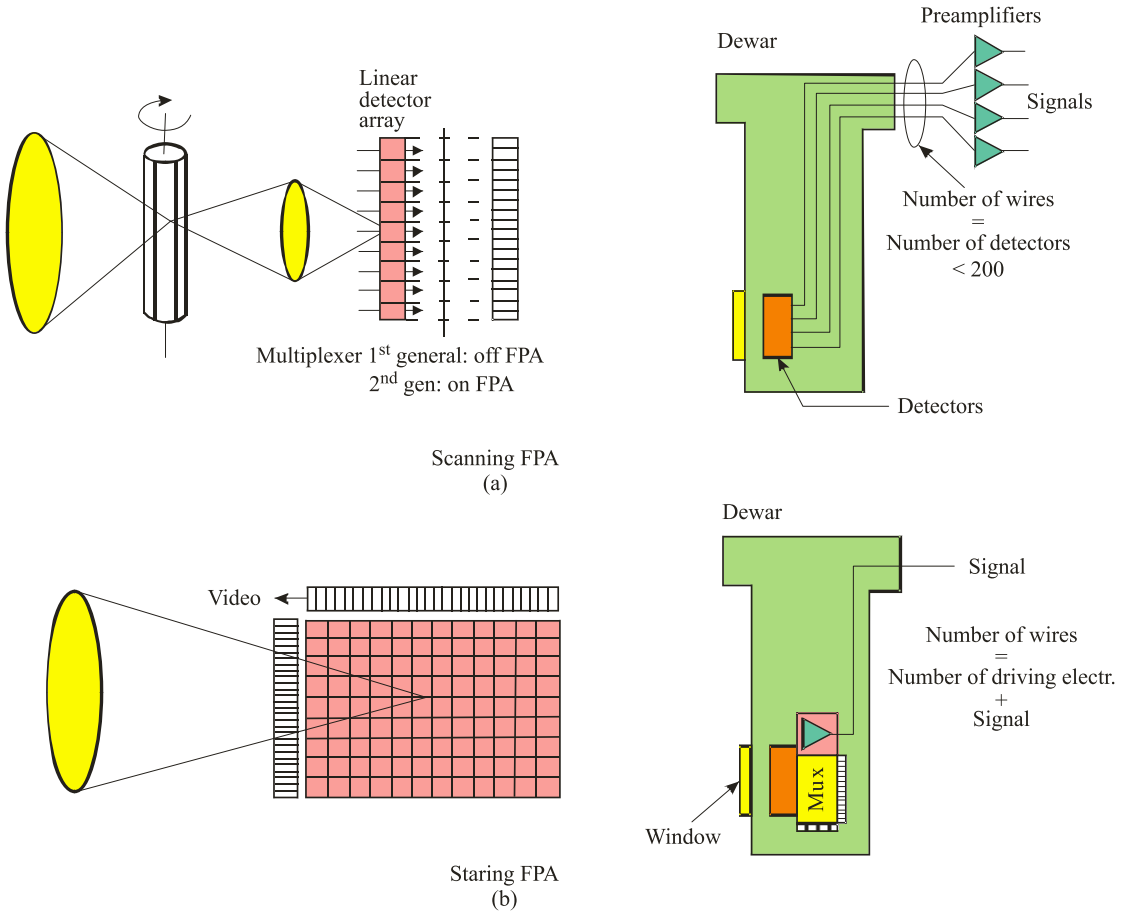

Fig. 20. (a) Scanning focal plane array (first generation) and (b) staring focal plane array (second generation).

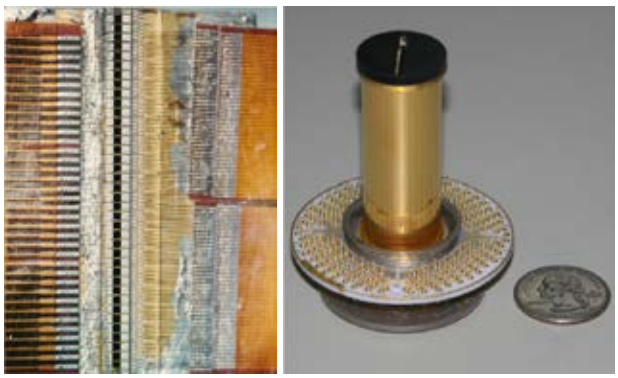

Fig. 21. A 180-element common module FPA mounted on a dewar stem (after Ref. 69).

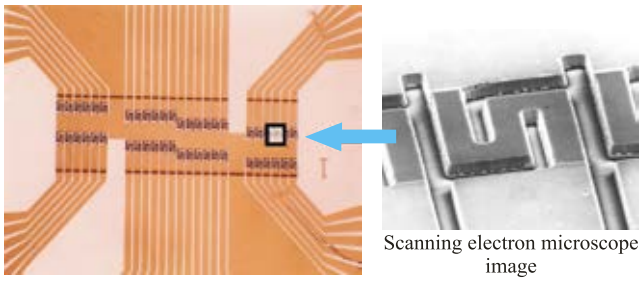

Fig. 22. Photomicrograph of 8×6 element photoconductive array of 50 μm square elements using labyrinthed structure for enhanced responsivity. Staggering the elements to solve the connection problems introduces delays between image lines (after Ref. 56).

A novel variation of the standard photoconductive device, the SPRITE detector (the acronym of Signal PRocessing In The Element), was invented in England [70,71]. A family of thermal imaging systems has utilized this device, however, now decline of its usage is observed. The SPRITE detector provides signal averaging of a scanned image spot what is accomplished by synchronization between the drift velocity of minority carriers along the length of photoconductive bar of material and the scan velocity of the imaging system. Then the image signal builds up a bundle of minority charge which is collected at the end of the photoconductive bar, effectively integrating the signal for a significant length of time and thereby improving the signal-to-noise ratio.

In the mid-seventies attention turned to the photodiodes for passive IR imaging applications. The main limitation of photoconductive detectors is that they cannot easily be multiplexed on the focal plane. In contrast to photoconductors, photodiodes with their very low power dissipation, inherently high impedance, negligible 1/*f* noise, and easy multiplexing on focal plane silicon chip, can be assembled in two-dimensional (2-D) arrays containing more than megapixel elements, limited only by existing technologies. These readout integrated circuits (ROICs) include, e.g., pixel deselecting, anti-blooming on each pixel, subframe imaging, output preamplifiers, and some other functions. Systems based upon such FPAs can be smaller, lighter with lower power consumption, and can result in a much higher performance that systems based on first generation detectors. Photodiodes can also have less low frequency noise, faster response time, and the potential for a more uniform spatial response across each element. However, the more complex processes needed for photovoltaic detectors have influenced on slower development and industrialization of the second generation systems. Another point is that, unlike photoconductors, there is a large variety of device structures with different passivations, junction-forming techniques and contact systems.

Intermediary systems are also fabricated with multiplexed scanned photodetector linear arrays in use and with, as a rule, time delay and integration (TDI) functions. The array illustrated in Fig. 22 is an 8×6 element photoconductive array elaborated in the middle 1970s and intended for use in a serial-parallel scan image. Staggering the elements to solve the connection problems introduces delays between image lines. Typical examples of modern systems are HgCdTe multilinear 288×4 arrays fabricated by Sofradir both for 3–5-μm and 8–10.5-μm bands with signal processing in the focal plane (photocurrent integration, skimming, partitioning, TDI function, output preamplification and some others).

After the invention of charge coupled devices (CCDs) by Boyle and Smith [53] the idea of an all-solid-state electronically scanned two-dimensional (2D) IR detector array caused attention to be turned to HgCdTe photodiodes. These include p-n junctions, heterojunctions, and MIS photo-capacitors. Each of these different types of devices has certain advantages for IR detection, depending on the particular application. More interest has been focused on the first two structures which can be reverse-biased for even higher impedance and can therefore match electrically with compact low-noise silicon readout preamplifier circuits. In the end of 1970s the emphasis were directed toward large photovoltaic HgCdTe arrays in the MW and LW spectral bands for thermal imaging. Recent efforts have been extended to short wavelengths, e.g. for starlight imaging in the short wavelength (SW) range, as well as to very LWIR (VLWIR) space borne remote sensing beyond 15 μm.

At present the most commonly used HgCdTe photodiode configurations are unbiased homo- (n^+-on-p) and heterojunction (P-on-n, P denotes the wider energy gap material) photodiodes. The n-on-p junctions are fabricated in two different manners using Hg vacancy doping and extrinsic doping. The use of Hg vacancy as p-type doping is known to kill the electron lifetime, and the resulting detector exhibits a higher current than in the case of extrinsic doping using As. Generally, n-on-p vacancy doped diodes give rather high diffusion currents but lead to a robust technology as its performance weakly depends on doping level and absorbing layer thickness. Due to higher minority carrier lifetime, extrinsic doping is used for low dark current (low flux) applications. The p-on-n structures are characterized by the lowest dark current.

Third generation HgCdTe systems are now being developed. These systems provide enhanced capabilities like larger number of pixels, higher frame rates, better thermal resolution as well as multicolour functionality and other on-chip functions. Multicolour capabilities are highly desirable for advanced IR systems. Systems that gather data in separate IR spectral bands can discriminate both absolute temperature and unique signatures of objects in the scene. By providing this new dimension of contrast, multiband detection also offers advanced colour processing algorithms to further improve sensitivity compared to that of single--colour devices.

The unit cell of integrated multicolour FPAs consists of several co-located detectors (see Fig. 6 – inside), each sensitive to a different spectral band. In the case of HgCdTe, this device architecture is realized by placing a longer wavelength HgCdTe photodiode optically behind a shorter wavelength photodiode. Each layer absorbs radiation up to its cut-off and hence transparent to the longer wavelengths, which are then collected in subsequent layers.

6. Alternative material systems

The difficulties in growing HgCdTe material, significantly due to solidus-liquidus separation and the high vapour pressure of Hg, encouraged the development of alternative technologies over the past fifty years. One of these was PbSnTe, mentioned previously [58,59]. InAs/$Ga_{1-x}In_xSb$ strained layer superlattices (SLSs) have been also proposed for IR detector applications in the 8–14-μm region [72]. Among different types of quantum well IR photodetectors (QWIPs) technology of the GaAs/AlGaAs multiple quantum well detectors is the most mature. The QWIP technology is relatively new that has been developed very quickly in the last decade [73–75] with LWIR imaging performance comparable to state of the art of HgCdTe. Below, the mentioned technologies are compared to HgCdTe ternary alloy one.

6.1. InSb and InGaAs

In the middle and late1950s it was discovered that InSb had the smallest energy gap of any semiconductor known at that time and its applications as middle wavelength infrared detector became obvious. The energy gap of InSb is less well matched to the 3–5-μm band at higher operating temperatures, and better performance can be obtained from HgCdTe. InAs is a similar compound to InSb, but has a larger energy gap, so that the threshold wavelength is 3–4-μm.

In InSb photodiode fabrication the standard manufacturing technique begins with bulk n-type single crystal wafers with donor concentration about 10^{15} cm^{-3} (the epitaxial techniques are used rarely). Relatively large bulk grown crystals with 3-in. and 4-in. diameters are available on the market. Figure 23 compares the dependence of dark current on temperature between HgCdTe and InSb photodiodes. This comparison suggests that MWIR HgCdTe photodiodes

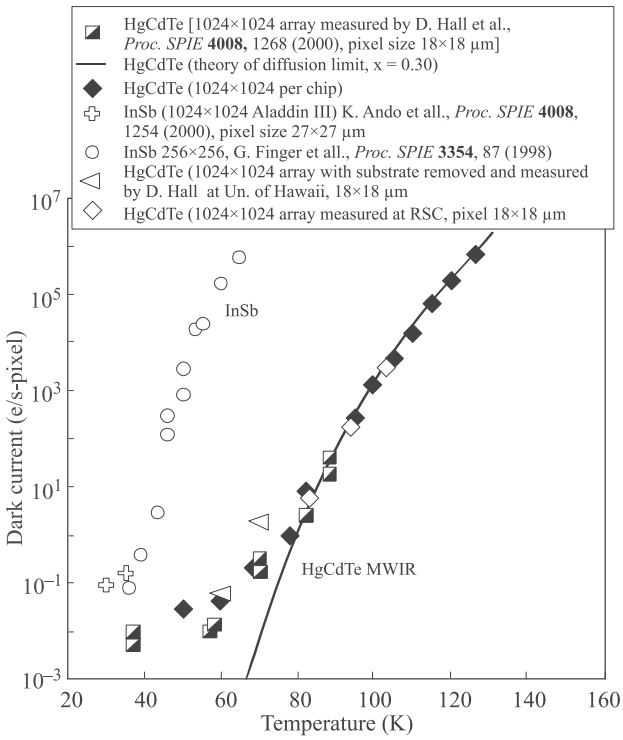

Fig. 23. The comparison of dependence of dark current on temperature between MBE-grown MWIR HgCdTe FPAs and highest reported value for InSb arrays. The HgCdTe 1024×1024 arrays with 18×18 μm pixels. The HgCdTe cutoff is 5.3 μm, and no AR coating, quantum efficiency is 73% at 78K (after Ref. 76).

have significant higher performance in the 30–120 K temperature range. The InSb devices are dominated by generation-recombination currents in the 60–120 K temperature range because of a defect centre in the energy gap, whereas MWIR HgCdTe detectors do not exhibit g-r currents in this temperature range and are limited by diffusion currents. In addition, wavelength tunability has made of HgCdTe the preferred material.

$In_{0.53}Ga_{0.47}As$ alloy (E_g = 0.73 eV, λ_c = 1.7 μm) lattice matched to the InP substrate is a suitable detector material for near-IR (1.0–1.7-μm) spectral range. Having lower dark current and noise than indirect-bandgap germanium, the competing near-IR material, the material is addressing both entrenched applications including lightwave communication systems, low light level night vision, and new applications such as remote sensing, eye-safe range finding and process control. Due to similar band structure of InGaAs and HgCdTe ternary alloys, the ultimate fundamental performance of both type of photodiodes are similar in the wavelength range of $1.5 < \lambda < 3.7$ μm [77]. InGaAs photodiodes have shown high device performance close to theoretical limits for material whose composition is nearly matched to that of InP (≅ 1.7 μm cut-off wavelength) and InAs (≅ 3.6 μm cut-off wavelength). However, the performance of InGaAs photodiodes decreases rapidly at intermediate wavelengths due to substrate lattice mismatch-induced defects.

Standard $In_{0.53}Ga_{0.47}As$ photodiodes have detector-limited room temperature detectivity of ~10^{13} cmHz$^{1/2}$W^{-1}. With increasing cutoff wavelength detectivity decreases.

6.2. GaAs/AlGaAs quantum well superlattices

Alternative hybrid detector for the long wavelength IR region (8–14-μm) are the quantum well infrared photoconductors (QWIPs). These high impedance detectors are built from alternating thin layers (superlattices) of GaAs and AlGaAs. Despite large research and development efforts, large photovoltaic LWIR HgCdTe FPAs remain expensive, primarily because of the low yield of operable arrays. The low yield is due to sensitivity of LWIR HgCdTe devices to defects and surface leakage, which is a consequence of basic material properties. With respect to HgCdTe detectors, GaAs/AlGaAs quantum well devices have a number of advantages, including the use of standard manufacturing techniques based on mature GaAs growth and processing technologies, highly uniform and well-controlled MBE growth on greater than 6 in. GaAs wafers, high yield and thus low cost, more thermal stability, and intrinsic radiation hardness.

LWIR QWIP cannot compete with HgCdTe photodiode as the single device, especially at higher temperature operation (> 70 K) due to fundamental limitations associated with intersubband transitions. QWIP detectors have relatively low quantum efficiencies, typically less than 10%. The spectral response band is also narrow for this detector, with a full-width, half-maximum of about 15%. All the QWIP detectivity data with cutoff wavelength about 9 μm is clustered between 10^{10} and 10^{11} cmHz$^{1/2}$/W at about 77 K operating temperature. However, the advantage of HgCdTe is less distinct in temperature range below 50 K due to the problems involved in an HgCdTe material (p-type doping, Shockley-Read recombination, trap-assisted tunnelling, surface and interface instabilities). A more detailed comparison of both technologies has been given by Rogalski [74] and Tidrow *et al.* [78]. Table 2 compares the essential properties of three types of devices at 77 K.

Even though that QWIP is a photoconductor, several of its properties such as high impedance, fast response time, long integration time, and low power consumption well comply with the requirements of large FPAs fabrication. The main drawbacks of LWIR QWIP FPA technology are the performance limitation for short integration time applications and low operating temperature. Their main advantages are linked to performance uniformity and to availability of large size arrays. The large industrial infrastructure in III–V materials/device growth, processing, and packaging brought about by the utility of GaAs-based devices in the telecommunications industry gives QWIPs a potential advantage in producibility and cost. The only known use of HgCdTe, to the date is for IR detectors. The main drawback of LWIR HgCdTe FPA technology is the unavailability of large size arrays necessary for TV format and larger formats.

6.3. InAs/GaInSb strained layer superlattices

The three semiconductors InAs, GaSb, and AlSb form an approximately lattice-matched set around 6.1 Å, with (room temperature) energy gaps ranging from 0.36 eV (InAs) to 1.61 eV (AlSb). Their heterostructures combining InAs with the two antimonides offers band lineups that are drastically different from those of the more widely studied AlGaAs system. The most exotic lineup is that of InAs/GaSb heterojunctions with a broken gap lineup: at the interface the bottom of conduction band of InAs lines up below the top of the valence band of GaSb with a break in the gap of about 150 meV. In such a heterostructure, with partial overlapping of the InAs conduction band with the GaSb-rich solid solution valence band, electrons and holes are spatially separated and localized in self-consistent quantum wells formed on both sides of the heterointerface. This leads to unusual tunnelling-assisted radiative recombination transitions and novel transport properties. From the viewpoint of producibility, III-V materials offer much stronger chemical bonds and thus higher chemical stability compared to HgCdTe. The 6.1 Å materials can be epitaxially grown on GaSb and InAs substrates. In particular, 4-inch diameter GaSb substrates became commercially available in 2009 offering improved economy of scale for fabrication of large format FPAs arrays.

InAs/$Ga_{1-x}In_xSb$ (InAs/GaInSb) strained layer superlattices (SLSs) are an alternative to the HgCdTe. The InAs/GaInSb material system is however in an early stage of development. Problems exist in material growth, processing, substrate preparation, and device passivation. Optimi-

Table 2. Essential properties of LWIR HgCdTe, type II SL photodiodes, and QWIPs at 77 K

Parameter	HgCdTe	QWIP (n-type)	InAs/GaInSb SL
IR absorption	Normal incidence	$E_{optical} \perp$ plane of well required Normal incidence: no absorption	Normal incidence
Quantum efficiency	≥ 70%	≤ 10%	≈ 30–40%
Spectral sensitivity	Wide-band	Narrow-band (FWHM ≈ 1 μm)	Wide-band
Optical gain	1	0.2–0.4 (30–50 wells)	1
Thermal generation lifetime	≈ 1 μs	≈ 10 ps	≈ 0.1 μs
R_oA product (λ_c = 10 μm)	10^3 Ω cm^2	10^4 Ω cm^2	10^3 Ω cm^2
Detectivity (λ_c = 10 μm, FOV = 0)	2×10^{12} cmHz$^{1/2}$W^{-1}	2×10^{10} cmHz$^{1/2}$W^{-1}	1×10^{12} cmHz$^{1/2}$W^{-1}

zation of SL growth is a trade-off between interface roughness, with smoother interfaces at higher temperature, and residual background carrier concentrations, which are minimized on the low end of this range.

The staggered band alignment of type-II superlattice shown in Fig. 24(a) creates a situation in which the energy band gap of the superlattice can be adjusted to form either a semimetal (for wide InAs and GaInSb layers) or a narrow band gap (for narrow layers) semiconductor material. The band gap of the SL is determined by the energy difference between the electron miniband E_1 and the first heavy hole state HH_1 at the Brillouin zone centre and can be varied continuously in a range between 0 and about 250 meV. One advantage of using type-II superlattice in LW and VLWIR is the ability to fix one component of the material and vary the other to tune wavelength. An example of the wide tunability of the SL is shown in Fig. 24(b).

In the SL, the electrons are mainly located in the InAs layers, whereas holes are confined to the GaInSb layers. This suppresses Auger recombination mechanisms and thereby enhances carrier lifetime. However, the promise of Auger suppression has not yet to be observed in practical device material. At present time, the measured carrier lifetime is below 100 ns and is limited by Shockley-Read mechanism in both MWIR and LWIR compositions. It is interesting to note that InSb has had a similar SR lifetime issue since its inception in 1950s. In a typical LWIR superlattice, the doping density is on the order of 1 to 2×10^{16} cm^{-3}, which is considerably higher than the doping level found in the LWIR HgCdTe (typically low 10^{15} cm^{-3}). This is possible because of tunnelling current suppression in superlattices. The higher doping compensates for the shorter lifetime, resulting in relatively low diffusion dark current at the expense of higher device capacitance.

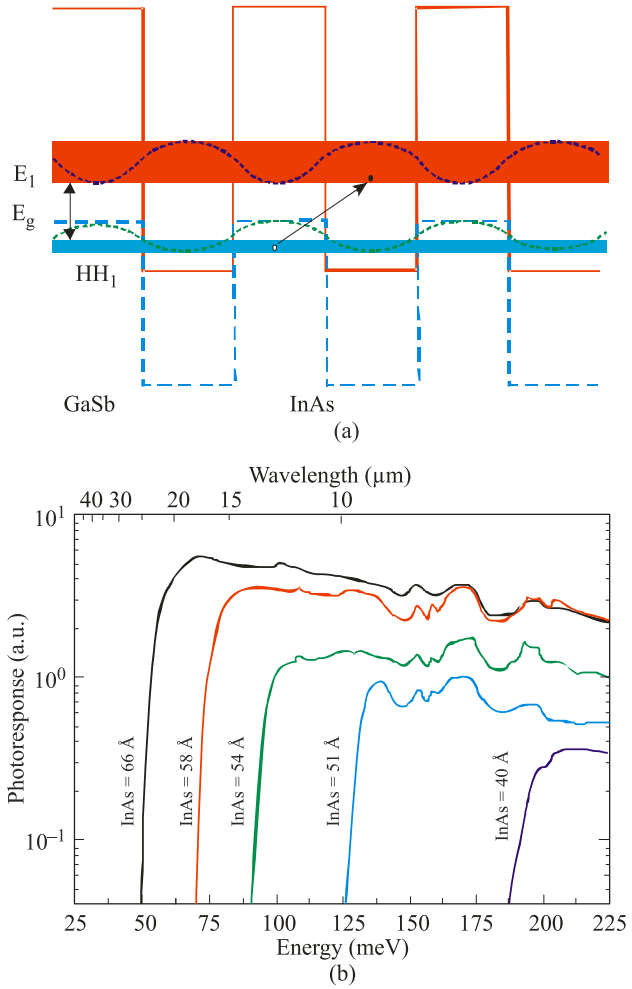

Fig. 24. InAs/GaSb strained layer superlattice: (a) band edge diagram illustrating the confined electron and hole minibands which form the energy bandgap; (b) experimental data of type II SLS cut-off wavelengths change with the InAs thickness while GaSb is fixed at 40 Å (after Ref. 79).

6.4. Hg-based alternatives to HgCdTe

Among the small gap II-VI semiconductors for infrared detectors, only $Hg_{1-x}Zn_xTe$ (HgZnTe) and $Hg_{1-x}Mn_xTe$ (HgMnTe) [80] can be considered as alternatives to HgCdTe. However, both ternary alloy systems have never been systematically explored in the device context. The reasons for this are several. Preliminary investigations of these alloy systems came on the scene when development of HgCdTe detectors was well on its way. Moreover, the HgZnTe alloy is a more serious technological problem material than HgCdTe. In the case of HgMnTe, Mn is not a group II element, so that HgMnTe is not a truly II–VI alloy. This ternary compound was viewed with some suspicion by those not directly familiar with its crystallographic, electrical and optical behaviour. In such a situation, proponents of parallel development of HgZnTe and HgMnTe for infrared detector fabrication encountered considerable difficulty in selling the idea to industry and to funding agencies.

7. New revolution in thermal detectors

As it was mentioned previously, the development of IR technology has been dominated by photon detectors since about 1930. However, photon detectors require cryogenic cooling. This is necessary to prevent the thermal generation of charge carriers. The thermal transitions compete with the optical ones, making non-cooled devices very noisy. The cooled thermal camera usually uses a Sterling cycle cooler, which is the expensive component in the photon detector IR camera, and the cooler's life time is only around 10000 hours. Cooling requirements are the main obstacle to the widespread use of IR systems based of semiconductor photon detectors making them bulky, heavy, expensive and inconvenient to use.

The use of thermal detectors for IR imaging has been the subject of research and development for many decades. However, in comparison with photon detectors, thermal detectors have been considerably less exploited in commercial and military systems. The reason for this disparity is that thermal detectors are popularly believed to be rather slow and insensitive in comparison with photon detectors.

As a result, the worldwide effort to develop thermal detectors has been extremely small in comparison with that of photon detector.

It must not be inferred from the preceding outline that work on thermal detectors has not also been actively pursued. Indeed, some interesting and important developments have taken place along this line. In 1947, for example, Golay constructed an improved pneumatic infrared detector [81]. This gas thermometer has been used in spectrometers. The thermistor bolometer, originally developed by Bell Telephone Laboratories, has found widespread use in detecting radiation from low temperature sources [82,83]. The superconducting effect has been used to make extremely sensitive bolometers.

Thermal detectors have also been used for infrared imaging. Evaporographs and absorption edge image converters were among the first non-scanned IR imagers. Originally an evaporograph was employed in which the radiation was focused onto a blackened membrane coated with a thin film of oil [84]. The differential rate of evaporation of the oil was proportional to radiation intensity. The film was then illuminated with visible light to produce an interference pattern corresponding to the thermal picture. The second thermal imaging device was the absorption edge image converter [85]. Operation of the device was based upon utilizing the temperature dependence of the absorption edge of semiconductor. The performance of both imaging devices was poor because of the very long time constant and the poor spatial resolution. Despite numerous research initiatives and the attractions of ambient temperature operation and low cost potential, thermal detector technology has enjoyed limited success in competition with cooled photon detectors for thermal imaging applications. A notable exception is the pyroelectric vidicon (PEV) [86] that is widely used by firefighting and emergency service organizations. The pyroelectric vidicon tube can be considered analogously to the visible television camera tube except that the photoconductive target is replaced by a pyroelectric detector and germanium faceplate. Compact, rugged PEV imagers have been offered for military applications but suffer the disadvantage of low tube life and fragility, particularly the reticulated vidicon tubes required for enhanced spatial resolution. The advent of the staring focal plane arrays (FPAs), however, marked the development of devices that would someday make uncooled systems practical for many, especially commercial, applications.

In the beginning of the 1970s in the US research programmers started to develop uncooled infrared detectors for practical military applications [10]. The efforts were mainly concentrated on ferroelectric barium strontium titanate detectors [(BST) in Texas Instruments (TI)] and micromachined bolometer technology [Honeywell (Morristown, NJ)]. Vanadium oxide microbolometers developed by Honeywell were subsequently licensed to numerous others. As a result of the limitations of BST, TI began an independent microbolometer development based on amorphous silicon (a-Si) instead of VO_x.

Throughout the 1980's and early 1990's, many other companies developed devices based on various thermal detection principles and the second revolution in thermal imaging began in the last decade of the 20th century. Although thermal detectors have been little used in scanned imagers because of their slow response, they are currently of considerable interest for 2-D electronically addressed arrays where the bandwidth is low and the ability of thermal devices to integrate over a significant fraction of a frame time is an advantage [43]. The development of uncooled IR arrays capable to imaging scenes at room temperature has been an outstanding technical achievement. Much of the technology was developed under classified military contracts in the United States, so the public release of this information in 1992 surprised many in the worldwide IR community [87].

In the mid 1990s amorphous silicon technology was developed in other countries, especially in France. During this time, the big advantage of using a-Si was their fabrication in a silicon foundry. The VO_x technology was controlled by the US military and export license was required for microbolometer cameras that were sold outside the US. Today, VO_x bolometers can be also produced in a silicon foundry and both above reasons disappeared.

TI also developed a thin-film ferroelectric (TFFE) technology as a simple upgrade to overcome the limitations of BST. After Raytheon acquired TI's defence business, microbolometers captured an increasing share of the rapidly growing market. In 2004 Raytheon sold the TI uncooled IR group with its BST, TFFE, and microbolometer technologies to L-3 Communications, who eventually discontinued BST production in 2009. TFFE technology development was discontinued about the same time because of manufacturing difficulties (most ferroelectrics tend to lose their interesting properties as the thickness is reduced).

At present large scale integration combined with micromachining has been used for manufacturing of large 2-D arrays of uncooled IR sensors. This enables fabrication of low cost and high-quality thermal imagers. Although developed for military applications, low-cost IR imagers are used in nonmilitary applications such as: drivers aid, aircraft aid, industrial process monitoring, community services, firefighting, portable mine detection, night vision, border surveillance, law enforcement, search and rescue, etc.

Microbolometers are the dominant uncooled IR detector technology with more than 95% of the market in 2010. At present, VO_x microbolometer arrays are clearly the most used technology for uncooled detectors (see Fig. 25). VO_x is

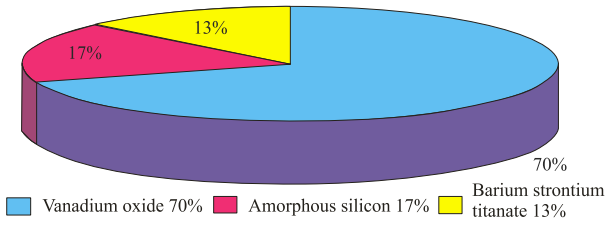

Fig. 25. Estimated market shares for VO_x, a-Si and BST detectors (after Ref. 88).

winner the battle between the technologies and VO_x detectors are being produced at a lower cost than either of the two other technologies [88]. However in the near future, VO_x will be challenged by a-Si material and new silicon based materials introduced by new market entrants, thanks to their cost structure, and easier manufacturability.

At present, the commercially available bolometer arrays are either made from VO_x, amorphous silicon (α-Si) or silicon diodes. Figure 26 shows scanning electron microscope (SEM) images of commercial bolometers fabricated by different manufacturers.

There is a strong system need to reduce the pixel size to achieve several important benefits. The detection range of many uncooled IR imaging systems is limited by pixel resolution rather than sensitivity. The development of highly sensitive small microbolometer pixels (e.g., 12-μm one), however, presents significant challenges in both fabrication process improvements and in pixel design. The current sensitivity (in A/W) of a scaled pixel may be improved by increasing the fill factor (*FF*), the absorption (ε), the thermal coefficient of the resistance (*TCR*), the applied voltage (V_{bias}) or by reducing the thermal conductance (G_{th}) or the resistance value of the thermistor (*R*), as it is shown by equation.

$$R_i = \frac{FF \cdot \varepsilon \cdot TCR \cdot V_{bias}}{G_{th} \cdot R}. \tag{8}$$

At the present stage of technology, the detector fill factor and the absorption coefficient are close to their ideal value and only a little benefit can be expected from the optimization of these two parameters. More gain can be obtained through improvement of the thermistor material; its *TCR* and *R*. A promising approach is the development of lower resistance a-Si/a-SiGe thin films [89,90]. The TCR of Si alloy has been increased to ≈3.9%/K from a baseline of 3.2%/K without an increase in material 1/*f*-noise. Amorphous-silicon technology is particularly susceptible to that, because it is capable of a *TCR* in excess of 5%/°C while maintaining its other excellent properties [91]. With this advantage, it is likely the a-Si microbolometer will soon establish itself as the premium technology for uncooled IR imaging. Also the properties of the Si/SiGe single crystalline quantum well as a thermistor material are promising [92].

8. Focal plane arrays – revolution in imaging systems

The term "focal plane array" (FPA) refers to an assemblage of individual detector picture elements ("pixels") located at the focal plane of an imaging system. Although the definition could include one-dimensional ("linear") arrays as well as two-dimensional (2D) arrays, it is frequently applied to the latter. Usually, the optics part of an optoelectronics imaging device is limited only to focusing of the image onto the detectors array. These so-called "staring arrays" are scanned electronically usually using circuits integrated with the arrays. The architecture of detector-readout assemblies has assumed a number of forms. The types of readout integrated circuits (ROICs) include the function of pixel deselecting, antiblooming on each pixel, subframe imaging, output preamplifiers, and may include yet other functions.

Detectors are only a part of usable sensor systems which include optics, coolers, pointing and tracking systems, electronics, communication, processing together with information-extraction sub-systems and displays (see Fig. 27) [93].

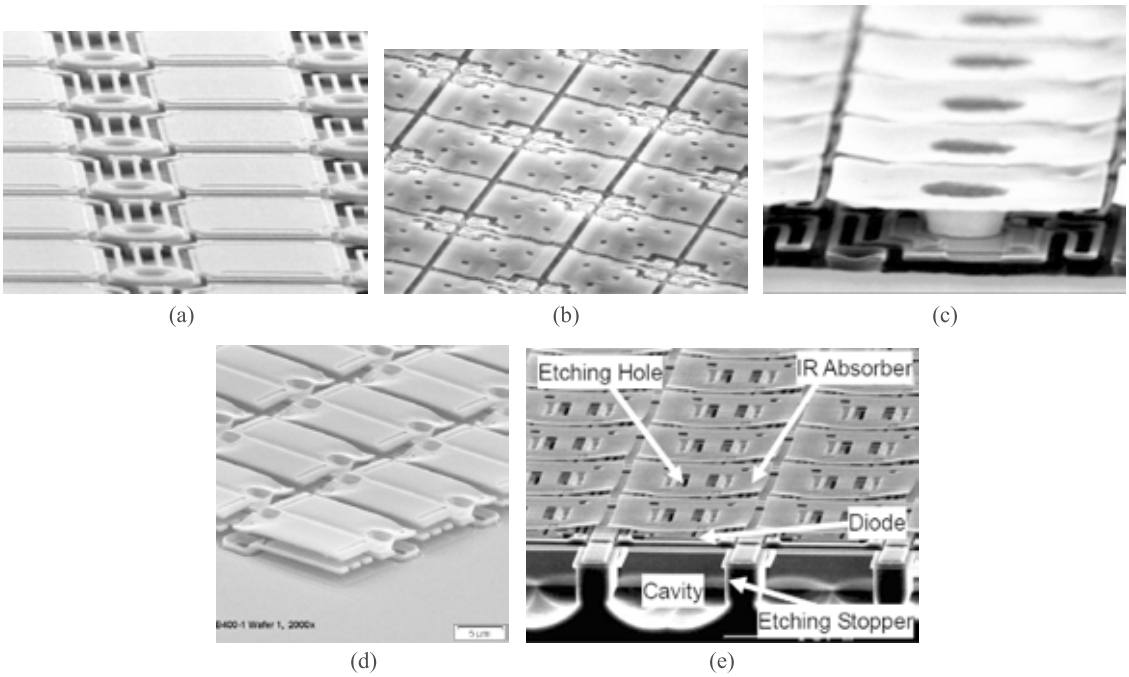

Fig. 26. Commercial bolometer design: (a) VO_x bolometer from BAE, (b) a-Si bolometer from Ulis, (c) VO_x umbrella design bolometer from DRS, (d) VO_x bolometer from Raytheon, and (e) SOI diode bolometer from Mitsubishi.

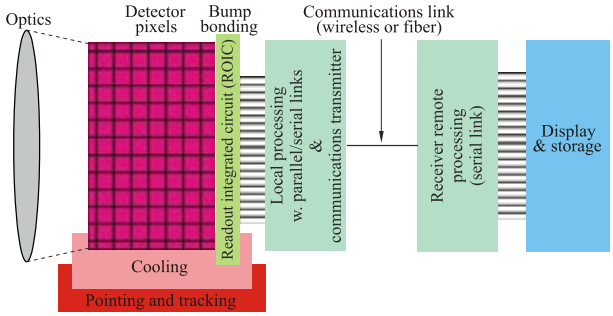

Fig. 27. Schematic representation of an imaging system showing important sub-systems (after Ref. 93).

So, the process of developing sensor system is significantly more challenging than fabricating a detector array.

In IR systems, 2-D arrays of detectors connected with indium bumps to a ROIC chip as a hybrid structure are often called a sensor chip assembly (SCA). The FPA industry is not sufficiently large to support the development of a complete set of unique tools. The evolution of the silicon industry can lead to divergence and to gaps in the FPA tool set. One simple example is that the silicon industry has standardized on a field size of 22×33 mm^2 for its lithography tools. The drive to larger pixel counts for FPAs often requires much larger overall FPA sizes which can only be accomplished by abutting multiple fields. Tiling large arrays from smaller chips addresses the practical and economic limits of making larger detector chips.

In the last four decades, different types of detectors are combined with electronic readouts to make detector arrays. The progress in integrated circuit design and fabrication techniques has resulted in continued rapid growth in the size and performance of these solid state arrays. In the infrared technique, these devices are based on a combination of a readout array connected to an array of detectors.

Development in detector focal plane array (FPA) technology has revolutionized many kinds of imaging [94]. From γ rays to the infrared and even radio waves, the rate at which images can be acquired has increased by more than a factor of a million in many cases. Figure 28 illustrates the trend in array size over the past 40 years. Imaging FPAs have developed in proportion to the ability of silicon inte-

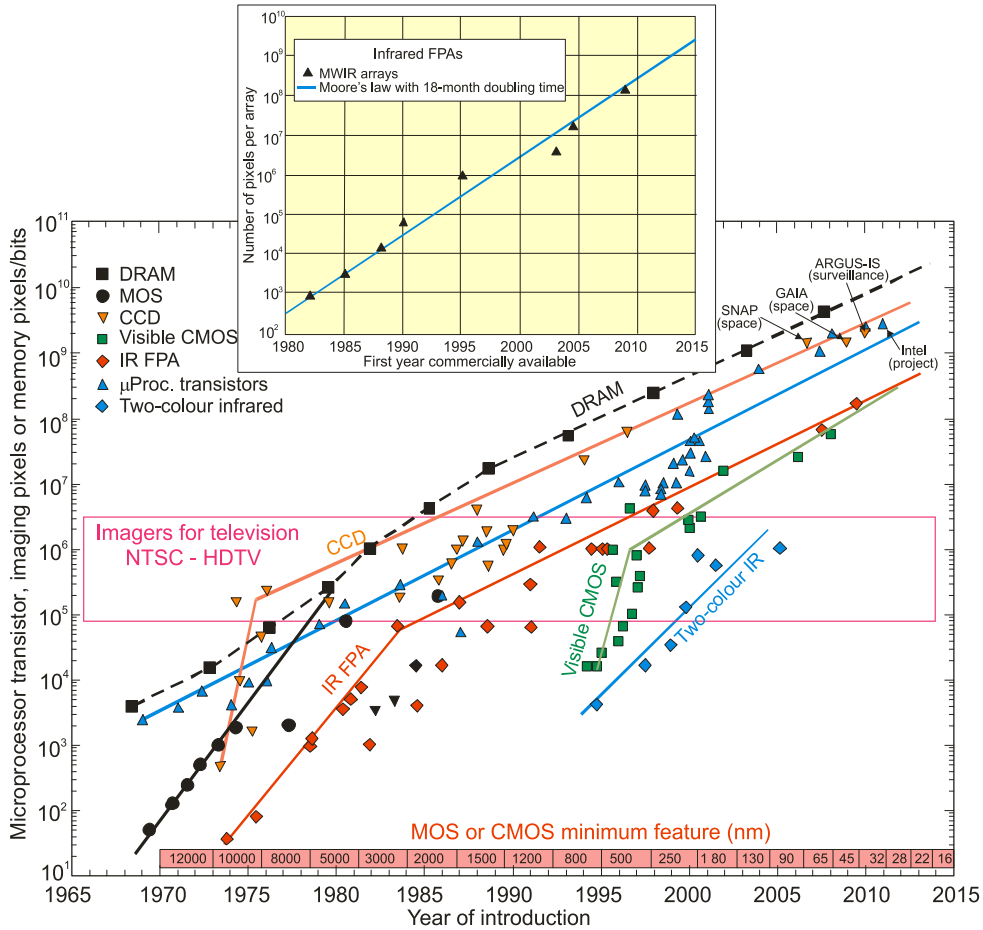

Fig. 28. Imaging array formats compared with the complexity of silicon microprocessor technology and dynamic access memory (DRAM) as indicated by transistor count and memory bit capacity (adapted after Ref. 94 with completions). The timeline design rule of MOS/CMOS features is shown at the bottom. CCDs with close to 2 gigapixels offer the largest formats. Note the rapid rise of CMOS imagers which are challenging CCDs in the visible spectrum. The number of pixels on an infrared array has been growing exponentially, in accordance with Moore's Law for 30 years with a doubling time of approximately 18 months. In infrared 147 mega pixel tiled mosaics are now available for astronomy applications. Imaging formats of many detector types have gone beyond that required for high definition TV.

grated circuit (ICs) technology to read and process the array signals, and with ability to display the resulting image. The progress in arrays has been steady and has paralleled the development of dense electronic structures such as dynamic random access memories (DRAMs). FPAs have nominally the same growth rate as DRAM ICs, which have had a doubling-rate period of approximately 18 months; it is a consequence of Moore's Low, but lag behind in size by about 5–10 years. The graph in insert of Fig. 28 shows the log of the number of pixels per a sensor chip assembly (SCA) as a function of the year first used on astronomy for MWIR SCAs. Charge coupled devices (CCDs) with close to 2 gigapixels offer the largest formats.

A number of architectures are used in the development of FPAs. In general, they may be classified as hybrid and monolithic, but these distinctions are often not as important as proponents and critics state them to be. The central design questions involve performance advantages versus ultimate producibility. Each application may favour a different approach depending on the technical requirements, projected costs and schedule.

In the case of hybrid technology (see Fig. 29), we can optimize the detector material and multiplexer independently. Other advantages of hybrid-packaged FPAs are near-100% fill factors and increased signal-processing area on the multiplexer chip. Development of hybrid packaging technology began in the late 1970's [95] and took the next decade to reach volume production (see Fig. 6). In the early 1990's, fully 2-D imaging arrays provided a means for staring sensor systems to enter the production stage. Recently, after hybridization, epoxy is wicked between the detector and the Si ROIC and the detector is thinned to 10 μm or less by diamond-point-turning. One important advantage of a thinned detector is that no substrate is needed; these detectors also respond in the visible portion of the spectrum.

8.1. Cooled FPAs

Although efforts have been made to develop monolithic structures using a variety of infrared detector materials (including narrow-gap semiconductors) over the past 40 years, only a few have matured to a level of practical use. These included PtSi, and more recently PbS, PbTe, and uncooled silicon microbolometers. Other infrared material systems (InGaAs, InSb, HgCdTe, GaAs/AlGaAs QWIP, and extrinsic silicon) are used in hybrid configurations. Table 3 contains a description of representative IR FPAs that are commercially available as standard products and/or catalogue items from the major manufacturers.

Figure 30 shows the timeline for HgCdTe FPA development at Raytheon Vision Systems (RVS, formerly Santa Barbara Research Center, SBRC). Advancements in IR sensor technology have enabled increased array sizes and decreased pixel sizes to facilitate the routine production of large megapixel arrays. The substrate size and corresponding detector array sizes started from the initial bulk HgCdTe crystal wafers of 3 cm^2, and progressed through LPE on CdZnTe substrates of 30 cm^2 up to today's MBE on alternate substrates of 180 cm^2.

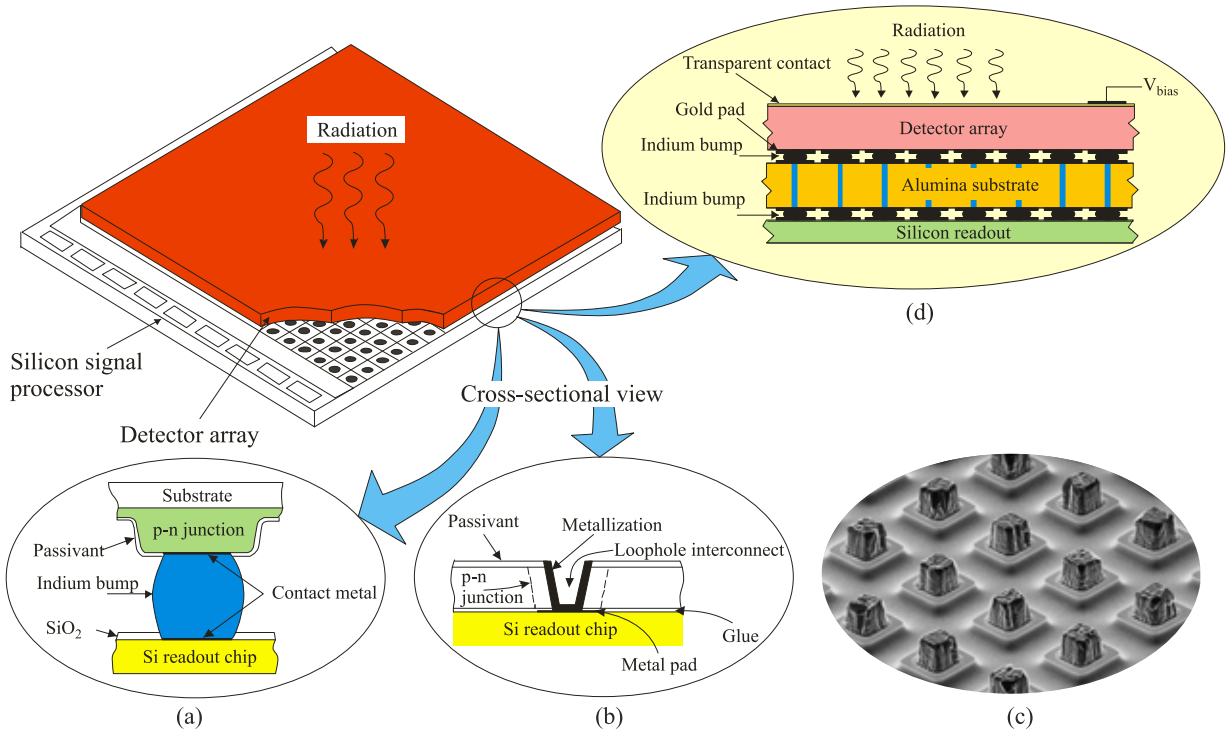

Fig. 29. Hybrid IR FPA interconnect techniques between a detector array and silicon multiplexer: (a) indium bump technique, (b) loophole technique, (c) SEM photo shows mesa photodiode array with indium bumps, and (d) layered-hybrid design suitable for large format far IR and sub-mm arrays.

Table 3. Representative IR FPAs offered by some major manufactures

Manufacturer/Web site	Size/Architecture	Pixel size (μm)	Detector material	Spectral range (μm)	Oper. temp. (K)	$D^*(\lambda_p)$ (cmHz$^{1/2}$/W)/ NETD (mK)
Goodrich Corporation www.sensorsinc.com	320×240/H	25×25	InGaAs	0.9–1.7	300	1×10^{13}
	640×512/H	25×25	InGaAs	0.4–1.7	300	$>6\times10^{12}$
Raytheon Vision Systems www.raytheon.com/businesses/ncs/rvs/index.html	1024×1024/H	30×30	InSb	0.6–5.0	50	
	2048×2048/H(Orion II)	25×25	HgCdTe	0.6–5.0	32	
	2048×2048/H(Virgo-2k)	20×20	HgCdTe	0.8–2.5	4–10	
	2048×2048/H	15×15	HgCdTe/Si	3.0–5.0	78	23
	1024×1024/H	25×25	Si:As	5–28	6.7	
	2048×1024/H	25×25	Si:As	5–28		
Teledyne Imaging Sensors http://teledynesi.com/imaging/	4096×4096/H(H4RG)	10×10 or 15×15	HgCdTe	1.0–1.7	120	
	4096×4096/H(H4RG)	10×10 or 15×15	HgCdTe	1.0–2.5	77	
	4096×4096/H(H4RG)	10×10 or 15×15	HgCdTe	1.0–5.4	37	
	2048×2048/H(H2RG)	18×18	HgCdTe	1.0–1.7	120	
	2048×2048/H(H2RG)	18×18	HgCdTe	1.0–2.5	77	
	2048×2048/H(H2RG)	18×18	HgCdTe	1.0–5.4	37	
Sofradir www.sofradir.com/	1000×256/H(Saturn)	30×30	HgCdTe	0.8–2.5	≤ 200	
	1280×1024/H(Jupiter)	15×15	HgCdTe	3.7–4.8	77–110	18
	384×288/H(Venus)	25×25	HgCdTe	7.7–9.5	77–80	17
	640×512/H	20×20	QWIP	8.0–9.0	73	31
	640×512/H	24×24	HgCdTe	MW(dual)	77–80	15–20
	640×512/H	24×24	HgCdTe	MW/LW(dual)	77–80	20–25
Selex www.selexsas.com/SelexGalileo/EN//index.sdo	1024×768/H(Merlin)	16×16	HgCdTe	3–5	up to 140	15
	640×512/H(Eagle)	24×24	HgCdTe	8–10	up to 90	24
	640×512/H(Condor)	24×24	HgCdTe	MW/LW(dual)	80	28/28
AIM www.aim-ir.com	640×512/H	24×24	HgCdTe	3–5		25
	640×512/H	15×15	HgCdTe	8–9		40
	384×288	40×40	Type II SL	MW(dual)		35/25
SCD www.scd.co.il	1280×1024/H	15×15	InSb	3–5	77	20
DRS Technologies www.drsinfrared.com	2048×2048/H	18×18	Si:As	5–28	7.8	
	1024×1024/H	25×25	Si:As	5–28	7.8	
	2048×2048/H	18×18	Si:Sb	5–40	7.8	

H – hybrid, M – monolithic

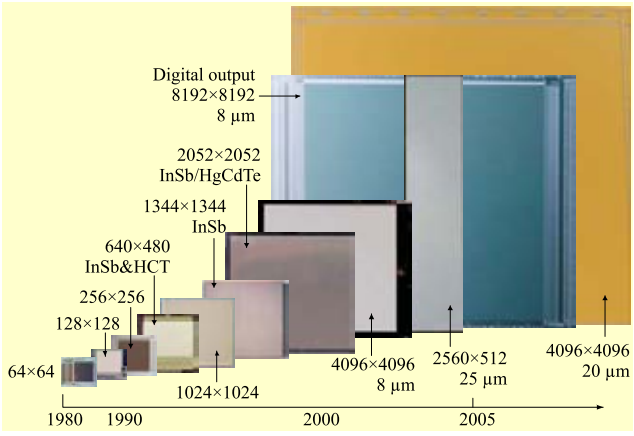

Fig. 30. Progression of ROIC format at RVS over time (after Ref. 96).

Pixel sizes as small as 10 μm have been demonstrated in hybrid systems. A general trend has been to reduce pixel sizes and this trend is expected to continue. Systems operating at sorter wavelengths are more likely to benefit from small pixel sizes because of the smaller diffraction-limited spot size. Diffraction-limited optics with low f-numbers (e.g., *f*/1) could benefit from pixels on the order of one wavelength across; about 10 μm in the LWIR. Over sampling the diffractive spot may provide some additional resolution for smaller pixels, but this saturates quickly as the pixel size is decreased. Pixel reduction is mandatory also to cost reduction of a system (reduction of the optics diameter, dewar size and weight, together with the power and increase the reliability). The pitch of 15 μm is in production today at Sofradir and pitches of 10-μm and less will be scheduled in short term [see Fig. 31(a)] [97]. Also there is a strong system need to reduce the pixel size of microbolometer arrays

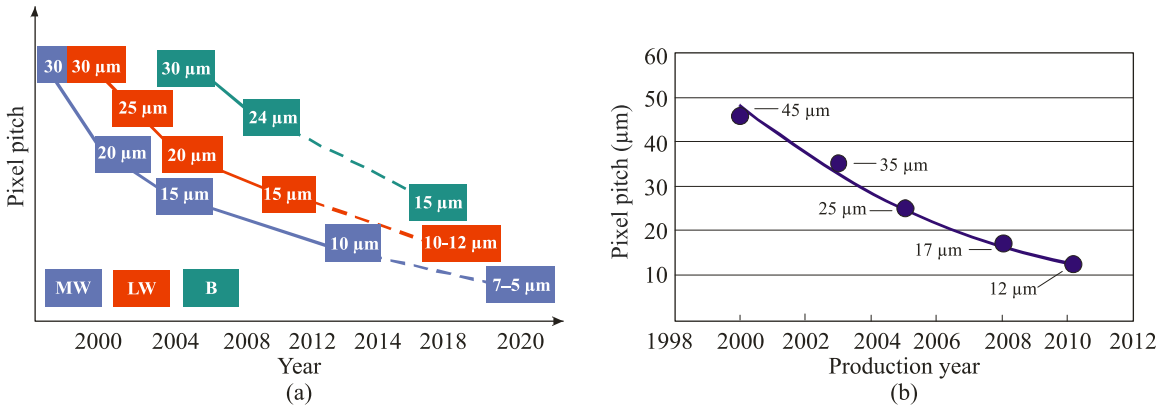

Fig. 31. Pixel pitch for HgCdTe photodiodes (a) (after Ref. 97) and amorphous silicon microbolometers (b) (after Ref. 98) have continued to decrease due to technological advancements.

to achieve several potential benefits [see Fig. 31(b)] [98]. The detection range of many uncooled IR imaging systems is limited by pixel resolution rather than sensitivity.

SWIR, MWIR and LWIR electronically scanned HgCdTe arrays with CMOS multiplexer are commercially available from several manufactures. Most manufactures produce their own multiplexer designs because these often have to be tailored to the applications. Figure 32 shows an example of large HgCdTe FPAs [98,99]. While the size of individual arrays continues to grow, the very large FPAs required for many space missions by mosaic-assembly of a large number of individual arrays. An example of a large mosaic developed by Teledyne Imaging Sensors, is a 147 megapixel FPA that is comprised of 35 arrays, each with 2048×2048 pixels [99].

In the last decade many manufacturers have made significant process improvements in the fabrication in both InSb detectors and readout electronic chips. The first InSb array to exceed one million pixels was the ALADDIN array first produced in 1993 by Santa Barbara Research Center (SBRC) and demonstrated on a telescope by National Optical Astronomy Observations (NOAO), Tucson, Arizona in 1994 [100]. This array had 1024×1024 pixels spaced on 27-µm centres and was divided into four independent quadrants, each containing 8 output amplifiers. A chronological history of the Raytheon Vision Systems (RVS) astronomical focal plane arrays is shown in Fig. 33 [101]. The next step in the development of InSb FPAs for astronomy was the 2048×2048 ORION SCA [102]. Four ORION SCAs were deployed as a 4096×4096 focal plane in the NOAO near-IR camera, currently in operation at the Mayall 4-meter telescope on Kitt Peak. Many of the packaging concepts used on the ORION program are shared with the 3-side buttable 2k×2k FPA InSb modules developed by RVS for the James Webb Space Telescope (JWST) mission. PHOENIX SCA is another 2k×2k FPA InSb array that has been fabricated and tested. This detector array is identical to ORION (25-µm pixels), however it readout is optimized for lower frames rates and lower power dissipation. With only 4 outputs the full frame read time is typically 10 seconds.

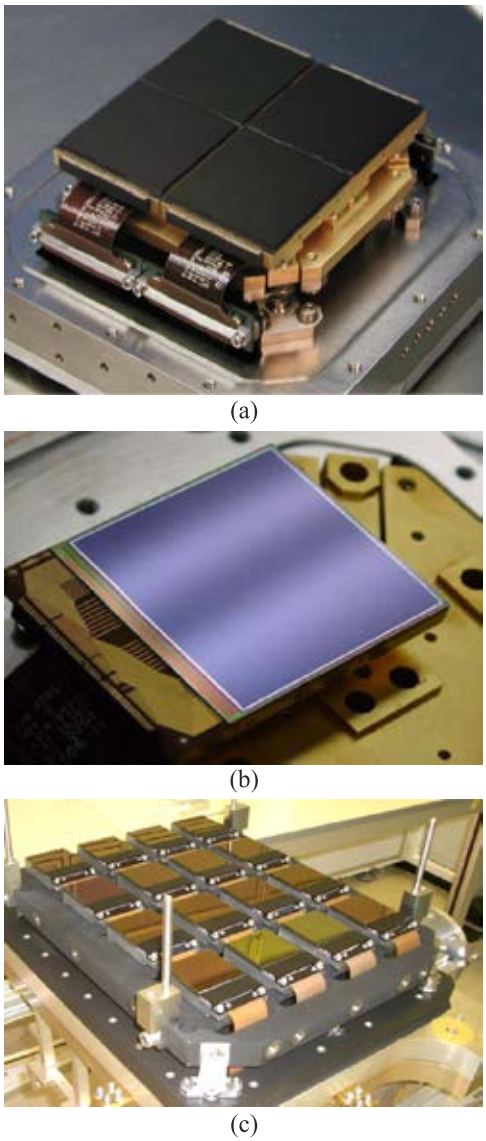

Fig. 32. Large HgCdTe FPAs: (a) a mosaic of four Hawaii-2RG-18 (4096×4096 pixels, 18-µm pitch), (b) Hawaii-4RG-10 (4096× 4096 pixels, 10-µm pitch) as is being used for astronomy observations (after Ref. 99), and (c) 16 2048×2048 HgCdTe arrays assembled for the VISTA telescope (after Ref. 98).

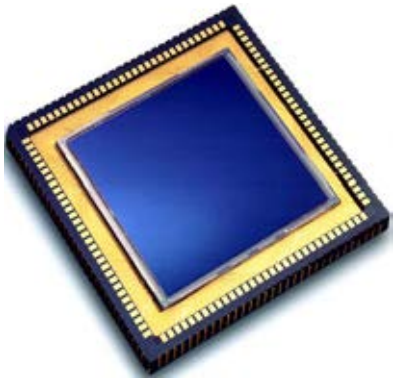

Aladdin: 1 k × 1 k
1994

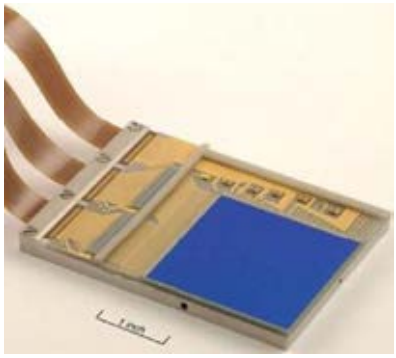

Orion: 2 k × 2 k
2001

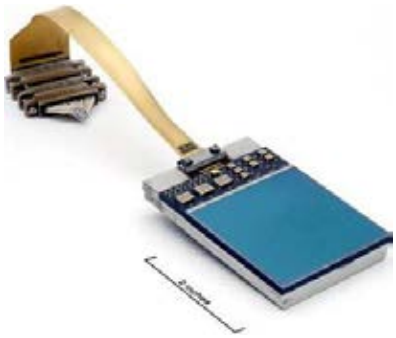

Phenix: 2 k × 2 k
2003

Fig. 33. Timeline and history development of the InSb RVS astronomy arrays (after Ref. 101).

State-of-the-art QWIP and HgCdTe FPAs provide similar performance figure of merit, because they are predominantly limited by the readout circuits. The very short integration time of LWIR HgCdTe devices of typically below 300 μs is very useful to freeze a scene with rapidly moving objects. The integration time of QWIP devices must be 10–100 times longer for that, and typically it is 5–20 ms [74]. Decision of the best technology is therefore driven by the specific needs of a system.

The blocked impurity band (BIB) devices, in large staring array formats are also now becoming commercially available. Impressive progress has been achieved especially in Si:As BIB array technology with formats as large as 2048×2048 and pixels as small as 18 μm; operated in spectral band up to 30 μm at about 10 K [103]. The pixel size of 18 μm is smaller than the wavelength at Q band (17–24 μm), however this does not pose any problem since an imager operating at these wavelengths will typically spread the beam out over many pixels to be fully sampled.

In the class of third generation systems, three detector technologies are now being developed: HgCdTe, QWIPs, and antimonide based type-II SLs. Two-colour FPAs are fabricated from multilayer materials using both sequential mode or simultaneous mode operations. The simplest two-colour HgCdTe detector and the first to be demonstrated was the bias selectable n-P-N triple-layer heterojunction (TLHJ), back-to-back photodiode shown in inside of Fig. 6 (capital letter means wider band gap structure). Many applications require true simultaneous detection in the two spectral bands. This has been achieved in a number of ingenious architectures considered in Ref. 104.

Large two-colour FPAs are fabricated by Raytheon, Sofradir, and Selex. RVS has developed two-colour, 1280×720 large format MWIR/LWIR FPAs with 20×20-μm unit cells [see Fig. 34(a)]. The ROICs share a common chip architecture and incorporate identical unit cell circuit designs and layouts; both FPAs can operate in either dual-band or single-band modes. Excellent high resolution IR camera imaging with *f*/2.8 FOV broadband refractive optics at 60 Hz frame rate has been achieved.

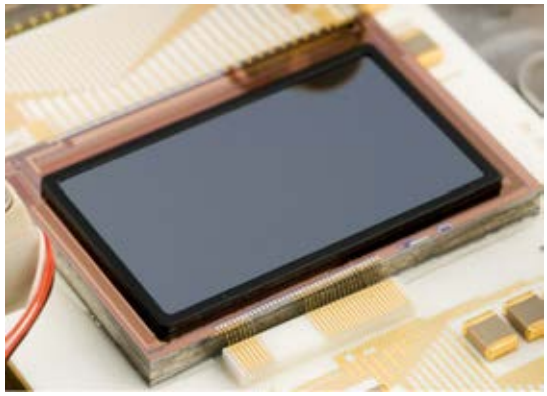

(a)

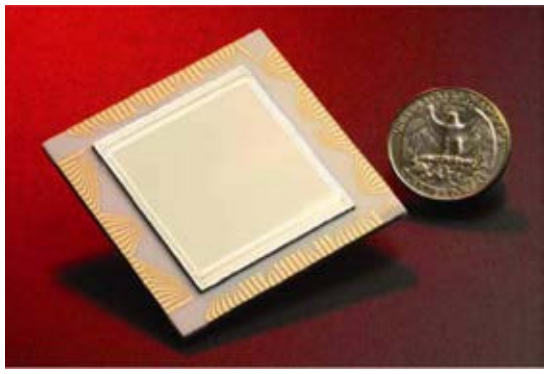

(b)

Fig. 34. Dual-band megapixel MW/LW FPAs: (a) RVS 1280×720 format HgCdTe FPAs mounted on dewar platforms (after Ref. 105), and (b) JPL 1024×1024 format QWIP FPA mounted on a 124-pin lead less chip carrier (after Ref. 106).

QWIPs are also ideal detectors for the fabrication of pixel co-registered simultaneously readable two-colour IR FPAs because a QWIP absorbs IR radiation only in a narrow spectral band and is transparent outside of that absorption band [107]. Thus, it provides zero spectral cross-talk when two spectral bands are more than a few microns apart.

Recently, type-II InAs/GaInSb SLs has emerged as a candidate for third generation IR detectors [108]. Over the past few years type-II superlattice based detectors have been also made rapid progress in fabrication of dual-band FPAs. Fraunhofer's dual-colour MWIR superlattice detector array technology with simultaneous, co-located detection capability is ideally suited for airborne missile threat warning systems [109]. Figure 35 illustrates a fully processed dual-colour 288×384 FPA. With 0.2 ms integration time and 78 K detector temperature, the superlattice camera achieves a temperature resolution of 29.5 mK for the blue channel (3.4 μm ≤ λ ≤ 4.1 μm) and 14.3 mK for the red channel (4.1 μm ≤ λ ≤ 5.1 μm).

As an example, the excellent imagery delivered by the 288×384 InAs/GaSb dual-colour camera is presented in Fig. 36. The image is a superposition of the images of the two channels coded in the complimentary colours cyan and red for the detection ranges of 3–4 μm and 4–5 μm, respectively. The red signatures reveal hot CO_2 emissions in the scene, whereas water vapour, e.g. from steam exhausts or in clouds appear cyan due to the frequency dependency of the Rayleigh scattering coefficient.

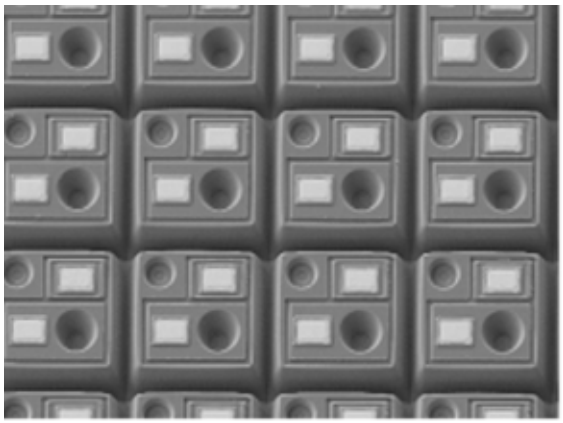

Fig. 35. SEM images illustrating the processing of 288×384 dual colour InAs/GaSb SLS FPAs. At a pixel pitch of 30 μm, three contact lands per pixel permit simultaneous and spatially coincident detection of both colours (after Ref. 109).

8.2. Uncooled FPAs

Initially developed for the military market by US defence companies, IR uncooled cameras are now widely used in many commercial applications. Currently, the microbolometer detectors are produced in larger volumes than all other IR array technologies together. Their cost will be drastically dropped (about –15% per year). It is expected that commercial applications in surveillance, automotive and thermography will reach total volumes more than 1,1 million units in 2016 ($3.4 B in value) (see Fig. 37) [110]. The present thermography boom is confirmed with camera prices now available for near $1,000 from FLIR that expand the use of IR cameras to maintenance engineers and building inspectors. Surveillance is becoming a key market with closed-circuit television (CCTV) big camera players introducing many new models of thermal cameras. In addition it is expected that automotive will exceed 500,000 units sales for 2016. Military uncooled camera markets are mainly driven by the huge US Military demand for soldiers (weapon sight, portable goggles, and vehicle vision enhancement). It takes more than 85% of the world market with a strong presence of DRS and BAE on various applications.

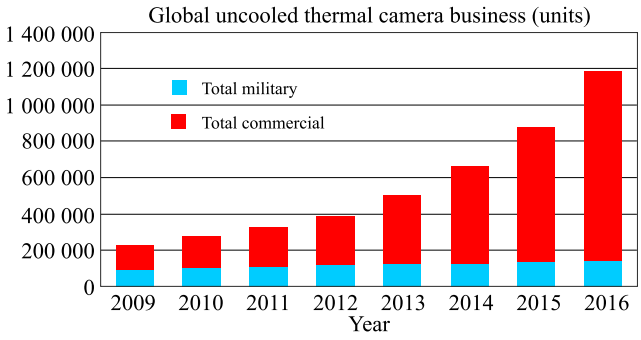

Fig. 37. Uncooled thermal camera business (units) (after Ref. 110).

Fig. 36. Bispectral infrared image of an industrial site taken with a 384×288 dual-colour InAs/GaSb SL camera. The two-colour channels 3–4 μm and 4–5 μm are represented by the complementary colours cyan and red, respectively (after Ref. 109).

Table 4. Representative commercial uncooled infrared bolometer array

Company	Bolometer type	Array format	Pixel pitch (μm)	Detector NEDT (mK) (f/1, 20–60 Hz)
L-3 (USA)	VO_x bolometer	320×240	37.5	50
www.l-3com.com	a-Si Bolometer	160×120 – 640×480	30	50
	a-Si/a-SiGe	320×240 – 1024×768	17	30–50
BAE (USA)	VO_x bolometer	320×240 – 640×480	28	30–50
http://www.baesystems.com	VO_x bolometer (standard design)	160×120 – 640×480	17	50
	VO_x bolometer (standard design)	1024×768	17	
DRS (USA)	VO_x bolometer (standard design)	320×240	25	35
www.drsinfrared.com	VO_x bolometer (umbrella design)	320×240	17	50
	VO_x bolometer (umbrella design)	640×480, 1024×768	17	
Raytheon (USA)	VO_x bolometer	320×240, 640×480	25	30–40
http://www.raytheon.com/	VO_x bolometer (umbrella design)	320×240, 640×480	17	50
capabilities/products/uncooled/	VO_x bolometer (umbrella design)	1024×480, 2048×1536	17	
ULIS (France)	a-Si Bolometer	160×120 – 640×480	25	<60
www.ulis-ir.com	a-Si Bolometer	640×480, 1024×768	17	<60
SCD (Israel)	VO_x bolometer	384×288	17	35
www.scd.co.il	VO_x bolometer	640×480	25	50
NEC (Japan)	VO_x bolometer	320×240	23.5	<75
http://www.nec.com	VO_x bolometer	640×480	23.5	<75

Table 4 contains an overview of the main suppliers and specifications for existing products and for bolometer arrays that are in the R&D stage. As it is shown, development of 17-μm pixel pitch FPAs is being extended to both smaller arrays (320×240) and arrays larger than 3 megapixels. Thermal image obtained with 1024×768 a-Si microbolometer detector shows both high sensitivity and resolution to as shown in Fig. 38(b). This device can detect temperature variations smaller than 50 mK.

Currently, the largest microbolometer array fabricated by Raytheon is shown on a wafer in Fig. 39. In the fabrication of 2048×1536 staring arrays and associated ROIC circuits, a stitching technique has been used. Each 200-mm wafer contains nine-2048×1536 uncooled detector die, which represents an 80% increase in yield over an equivalent 150 mm wafer.

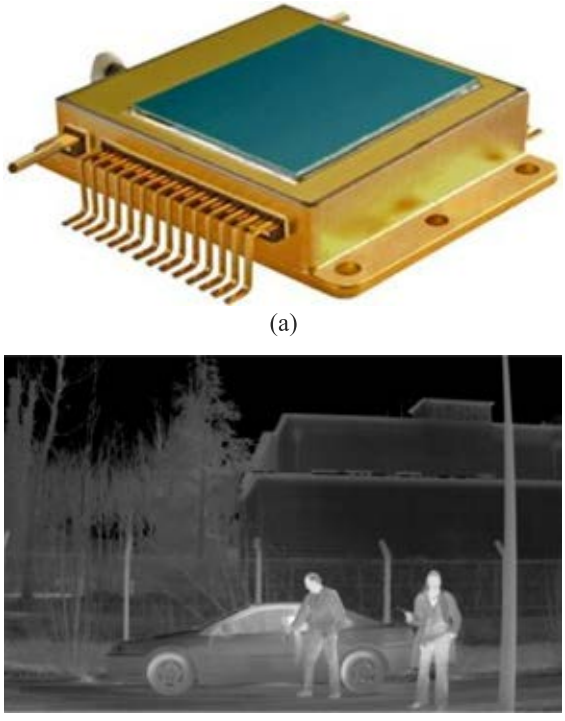

(a) (b)

Fig. 38. Ulis 17-μm pitch 1024×768 FPA: (a) packaging and (b) thermal image (after Ref. 111).

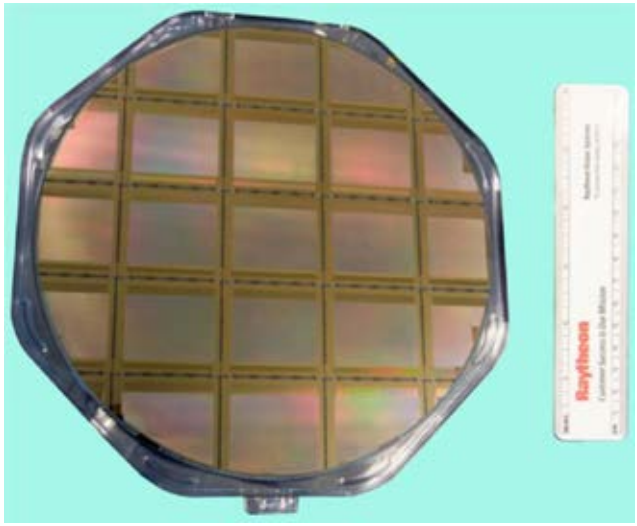

Fig. 39. 2048×1536 uncooled VO_x microbolometers with 17-μm pixel pitch on a 200 mm wafer (after Ref. 112).

8.3. Readiness level of LWIR detector technologies

We follow here after Ref. 93. Table 5 provides a snapshot of the current state development of LWIR detectors fabricated from different material systems. Note that TRL means technology readiness level. The highest level of TRL (ideal maturity) achieves value of 10. The highest level of maturity (TRL = 9) is credited to HgCdTe photodiodes and microbolometers. A little less, TRL = 8, for QWPs. The type-II InAs/GaInSb SL structure has great potential for LWIR spectral range application with performance comparable to HgCdTe for the same cutoff wavelength, but require a significant investment and fundamental material breakthrough to mature.

Quantum dot IR photodetector (QDIP) technology is at a very early stage of development (TRL = 1–2). The bias--dependent spectral response of this type of detector can be exploited to realize spectrally smart sensors whose wavelength and bandwidth can be tuned depending on the desired application. The main disadvantage of QDIPs is the large inhomogeneous linewidth of the QD ensemble variation of dot size in the Stranski-Krastanow growth mode. As a result, the absorption coefficient is reduced having a deleterious effect on QDIP performance [113].

9. Summary

This paper presents a historical look on IR detector developments from the beginning, discovery of infrared radiation by F.W. Herschel, to the present days. The years during World War II saw the origins of modern IR detector technology. Recent success in applying IR technology has been made possible by the successful development of high-performance infrared detectors over the last six decades. Interest has centred mainly on the wavelengths of the two atmospheric windows from 3–5 μm and 8–14 μm, though in recent years there has been an increasing interest in longer wavelengths stimulated by space applications. Demands to use these technologies are quickly growing due to their effective applications, e.g., in global monitoring of environmental pollution and climate changes, long time prognoses of agriculture crop yield, chemical process monitoring, Fourier transform IR spectroscopy, IR astronomy, car driving, IR imaging in medical diagnostics, and others.

Array sizes will continue to increase but perhaps at a rate that falls below the Moore's Law curve. An increase in array size is already technically feasible. However, the market forces that have demanded larger arrays are not as strong now that the megapixel barrier has been broken. Astronomers, in particular, have eagerly waited for the day when optoelectronic arrays could match the size of photographic film. Development of large format, high sensitivity, mosaic sensors for ground-based astronomy is the goal of many observatories around the world, since large arrays dramatically multiply the data output of a telescope system.

At present HgCdTe is the most widely used semiconductor material for IR photodetectors. It is predicted that HgCdTe technology will continue in the future to expand the envelope of its capabilities because of its excellent properties. Despite serious competition from alternative technol-

Table 5. Comparison of LWIR existing state-of-the-art device systems for LWIR detectors (after Ref. 93).
Note: TRL - technology readiness level

	Bolometer	HgCdTe	Type-II SLs	QWIP	QDIP
Maturity	TRL 9	TRL 9	TRL 2–3	TRL 8	TRL 1–2
Status	Material of choice for application requiring medium to low performance	Material of choice for application requiring high performance	Research and development	Commercial	Research and development
Military system examples	Weapon sight, night vision goggles, missile seekers, small UAV sensors, unattended ground sensors	Missile intercept, tactical ground and air born imaging, hyper spectral, missile seeker, missile tracking, space based sensing	Being developed in university and evaluated industry research environment	Being evaluated for some military applications	Very early stages of development at universities
Limitations	Low sensitivity and long time constants	Performance susceptible to manufacturing variations. Difficult to extend to >14-μm cutoff	Requires a significant, > $100M, investment and fundamental material breakthrough to mature	Narrow bandwith and low sensitivity	Narrow bandwith and low sensitivity
Advantages	Low cost and requires no active cooling, leverages standard Si manufacturing equipment	Near theoretical performance, will remain material of choice for minimum of the next 10–15 years	Theoretically better then HgCdTe at >14-μm micron cut--off, leverages commercial III–V fabrication techniques	Low cost applications. Leverages commercial manufacturing processes. Very uniform material	Not sufficient data to characterize material advantages

ogies, HgCdTe is unlikely to be seriously challenged for high-performance applications, applications requiring multispectral capability and fast response. Only a relatively new alternative IR material system, InAs/GaInSb superlattice, has great potential for LWIR/VLWIR spectral ranges with performance comparable to HgCdTe with the same cutoff wavelength.

Quick application of civilian IR technology is mainly connected with powerful development of uncooled cameras. Currently, the microbolometer detectors are produced in larger volumes than all other IR array technologies together and it is predicted that this tendency will be increased in the future.

References

1. W. Herschel, "Experiments on the refrangibility of the invisible rays of the Sun," *Phil. Trans. Roy. Soc. London* **90**, 284–292 (1800).
2. http://coolcosmos.ipac.caltech.edu/sitemap.html#cosmicclassroom
3. E.S. Barr, "Historical survey of the early development of the infrared spectral region," *Amer. J. Phys.* **28**, 42–54 (1960).
4. E.S. Barr, "The infrared pioneers – I. Sir William Herschel," *Infrared Phys.* **1**, 1 (1961).
5. R.A. Smith, F.E. Jones, and R.P. Chasmar, *The Detection and Measurement of Infrared Radiation,* Clarendon, Oxford, 1958.
6. P.W. Kruse, L.D. McGlauchlin and R.B. McQuistan, *Elements of Infrared Technology,* Wiley, New York, 1962.
7. R.D. Hudson, *Infrared System Engineering*, Wiley-Interscience, New Jersey, 1969.
8. E.S. Barr, "The infrared pioneers – II. Macedonio Melloni," *Infrared Phys.* **2**, 67–73 (1962).
9. E.S. Barr, "The Infrared Pioneers – III. Samuel Pierpont Langley," *Infrared Phys.* **3**, 195–206 (1963).
10. L.M. Biberman and R.L. Sendall, "Chapter 1. Introduction: A brief history of imaging devices for night vision," in *Electro-Optical Imaging: System Performance and Modeling*, edited by L.M. Biberman, pp. 1-1–1-26, SPIE Press, Bellingham, 2000.
11. J. Caniou, *Passive Infrared Detection: Theory and Application*, Kluwer Academic Publishers, Dordrecht, 1999
12. K. Herrmann and L. Walther, *Wissensspeicher Infrarottechnik* (*Store of Knowledge in Infrared Technology*), Fachbuchverlag, Leipzig, 1990.
13. T.J. Seebeck, "Magnetische Polarisation der Metalle und Erze durch Temperatur-Differenz," *Abh. Deutsch. Akad. Wiss. Berlin*, 265–373 (1822).
14. http://catalogue.museogalileo.it/section/ElectricityMagnetism.html.
15. http://earthobservatory.nasa.gov/Features/Langley/langley_2.php.
16. S.P. Langley, "The bolometer and radiant energy," *Proc. Am. Academy of Arts and Sciences* **16**, 342–358 (May 1880 – Jun. 1881).
17. C.D. Walcott, *Samuel Pierpont Langley*, City of Washington, The National Academy of Science, April, 1912.
18. W. Smith, "Effect of light on selenium during the passage of an electric current," *Nature* **7**, 303 (1873).
19. M. F. Doty, *Selenium, List of References, 1917–1925,* New York Public Library, New York, 1927.
20. *Applied Optics* (November, 1963), commemorative issue with extensive material on Coblentz's scientific work
21. W.F. Meggers, *William Weber Coblentz.1873–196*, National Academy of Science, Washingthon, 1967.
22. H. Hertz, "Ueber den Einfluss des ultravioletten Lichtes auf die electrische Entladung," *Annalen der Physik* **267**(8) 983–1000 (1887).
23. J. Elster, H. Geitel, "Ueber die Entladung negativ electrischer Körper durch das Sonnen- und Tageslicht," Ann. Physik 497–514 (1889).
24. F. Braun, "Uber die Stromleitung durch Schwefelmetalic," *Annalen der Physik and Chemie* **153**(4), 556–563 (1874).
25. J. C. Bose, "Detector for electrical disturbances," *U. S. Patent 755,840* (Filed September 30, 1901. Issued March 29, 1904).
26. T.W. Case, "Notes on the change of resistance of certain substrates in light," *Phys. Rev.* **9**, 305–310 (1917).
27. S.F. Johnson, *A History of Light and Colour Measurement. Science in the Shadows*, IOP Publishing Ltd, Bristol, 2001.
28. T.W. Case, "The thalofide cell – a new photoelectric substance," *Phys. Rev*. **15**, 289 (1920).
29. G. Holst, J.H. de Boer, M.C. Teves, and C.F. Veenemans, "Foto-electrische cel en inrichting waarmede uit een primair, door directe lichtstralen gevormd beeld een geheel ofnagenoeg geheel conform secundair optisch beeld kan," Dutch Patent 27062 (1928), British Patent 326200; D.R.P. 535208; "An apparatus for the transformation of light of long wavelength into light of short wavelength," *Physica* **1**, 297–305 (1934).
30. L. Koller, "Photoelectric emission from thin films of caesium," *Phys. Rev*. **36**, 1639–1647 (1930); N.R. Campbell, "Photoelectric emission of thin films," *Phil. Mag*. **12**, 173–185 (1931).
31. A.M. Glover, "A review of the development of sensitive phototubes," *Proc. IRE*, 413–423, August 1941.
32. S. Asao and M. Suzuki, "Improvement of thin film caesium photoelectric tube," *Proc. Phys. Math. Soc*. (Japan, series 3), **12**, 247–250. October 1930.
33. V.P. Ponomarenko and A.M. Filachev, *Infrared Techniques and Electro-Optics in Russia: A History 1946-2006*, SPIE Press, Bellingham, 2007.
34. E. W. Kutzscher, "Review on detectors of infrared radiation," *Electro-Opt. Syst. Design* **5**, 30 (June 1973).
35. W.N. Arnquist, "Survey of early infrared developments," Proc. IRE 47 1420–1430 (1959).
36. R.J. Cushman, "Film-type infrared photoconductors," *Proc. IRE* **47**, 1471–1475 (1959).
37. D.J. Lovell, "Cashman thallous sulfide cell," *Appl. Opt*. **10**, 1003–1008 (1971).
38. D.J. Lovell, "The development of lead salt detectors," *Amer. J. Phys.* **37**, 467–478 (1969).
39. M. Judt and B. Ciesla, *Technology Transfer out of Germany after 1945*, Routledge Studies in the History of Science, Technology and Medicine, Overseas Publishers Association, Amsterdam, 1996.
40. P.R. Norton, "Infrared detectors in the next millennium," *Proc. SPIE* **3698**, 652–665 (1999)
41. A. Rogalski, *Infrared Detectors*, 2nd edition, CRC Press, Boca Raton, 2010.

42. R.C. Jones, "Phenomenological description of the response and detecting ability of radiation detectors," *Proc. IRE* **47**, 1495–1502 (1959).
43. P.W. Kruse, *Uncooled Thermal Imaging*, SPIE Press, Bellingham, 2001.
44. P. Norton, "Third-generation sensors for night vision," *Opto--Electron. Rev*. **14**, 1–10 (2006).
45. http://www.nvl.army.mil/history.html
46. "Sidewinder article", http://wiki.scramble.nl/index.php?title =Sidewinder_article
47. http://ookaboo.com/o/pictures/picture/21952750/Prototype _Sidewinder1_missile_on_an_AD4_
48. B.V. Rollin and E.L. Simmons, "Long wavelength infrared photoconductivity of silicon at low temperatures," *Proc. Phys. Soc*. **B65**, 995–996 (1952).
49. E. Burstein, J.J. Oberly, and J.W. Davisson, "Infrared photoconductivity due to neutral impurities in silicon," *Phys. Rev*. **89**(1), 331–332 (1953).
50. E. Burstein, G. Pines and N. Sclar, "Optical and photoconductive properties of silicon and germanium," in *Photoconductivity Conference at Atlantic City*, edited by R. Breckenbridge, B. Russell and E. Hahn, pp. 353–413, Wiley, New York, 1956.
51. S. Borrello and H. Levinstein, "Preparation and properties of mercury moped germanium," *J. Appl. Phys*. **33**, 2947–2950 (1962).
52. R. A. Soref, "Extrinsic IR potoconductivity of Si dped with B, Al, Ga, P, As or Sb," *J. Appl. Phys.* **38**, 5201–5209 (1967).
53. W.S. Boyle and G.E. Smith, "Charge-coupled semiconductor devices," *Bell Syst. Tech. J.* **49**, 587–593 (1970).
54. F. Shepherd and A. Yang, "Silicon Schottky retinas for infrared imaging," *IEDM Tech. Dig.,* 310–313 (1973).
55. W.D. Lawson, S. Nielson, E.H. Putley, and A.S. Young, "Preparation and properties of HgTe and mixed crystals of HgTe-CdTe," *J. Phys. Chem. Solids* **9**, 325–329 (1959).
56. T. Elliot, "Recollections of MCT work in the UK at Malvern and Southampton," *Proc. SPIE* 7298, 72982M (2009).
57. P.W. Kruse, M.D. Blue, J.H. Garfunkel, and W.D. Saur, "Long wavelength photoeffects in mercury selenide, mercury telluride and mercury telluride-cadmium telluride," *Infrared Phys.* **2**, 53–60, 1962.
58. J. Melngailis and T. C. Harman, "Single-crystal lead-tin chalcogenides," in *Semiconductors and Semimetals,* Vol 5, pp. 111–174, edited by R. K. Willardson and A. C. Beer, Academic Press, New York, 1970.
59. T.C. Harman and J. Melngailis, "Narrow gap semiconductors," in *Applied Solid State Science,* Vol. 4, pp. 1–94, edited by R. Wolfe, Academic Press, New York, 1974.
60. R. Dornhaus, G. Nimtz, and B. Schlicht, *Narrow Gap Semiconductors*, Springer, Berlin, 1983.
61. J. Baars, "New aspects of the material and device technology of intrinsic infrared photodetectors," in *Physics and Narrow Gap Semiconductors,* pp. 280–282, edited by E. Gornik, H. Heinrich and L. Palmetshofer, Springer, Berlin (1982).
62. J.T. Longo, D.T. Cheung, A.M. Andrews, C.C. Wang, and J.M. Tracy, "Infrared focal planes in intrinsic semiconductors," *IEEE Trans. Electr. Dev.* **ED–25**, 213–232 (1978).
63. D. Long and J.L. Schmit, "Mercury-cadmium telluride and closely related alloys," in *Semiconductors and Semimetals,* Vol. 5, pp. 175–255, edited by R. K. Willardson and A. C. Beer, Academic Press, New York (1970).
64. P. Norton, "HgCdTe infrared detectors," *Opto-Electron. Rev.* **10**, 159–174 (2002).
65. C. Verie and R. Granger, "Propriétés de junctions p-n d'alliages $Cd_xHg_{1-x}Te$," *C. T. Acad. Sc.* **261**, 3349–3352 (1965).
66. G.C. Verie and M. Sirieix, "Gigahertz cutoff frequency capabilities of CdHgTe photovoltaic detectors at 10.6 μm," *IEEE J. Quant. Electr.* **8**, 180–184 (1972).
67. B.E. Bartlett, D.E. Charlton, W.E. Dunn, P.C. Ellen, M.D. Jenner, and M.H. Jervis, "Background limited photoconductive detectors for use in the 8–14 micron atmospheric window," *Infrared Phys.* **9**, 35–36 (1969).
68. M.A. Kinch, S.R. Borrello, and A. Simmons, "0.1 eV HgCdTe photoconductive detector performance," *Infrared Phys.* **17**, 127–135 (1977).
69. M.A. Kinch, "Fifty years of HgCdTe at Texas Instruments and beyond," *Proc. SPIE* **7298**, 72982T (2009).
70. C.T. Elliott, D. Day, and B.J. Wilson, "An integrating detector for serial scan thermal imaging," *Infrared Physics* **22**, 31–42 (1982).
71. A. Blackburn, M.V. Blackman, D.E. Charlton, W.A.E. Dunn, M.D. Jenner, K.J. Oliver, and J.T.M. Wotherspoon, "The practical realization and performance of SPRITE detectors," *Infrared Phys.* **22**, 57–64 (1982).
72. D. L. Smith and C. Mailhiot, "Proposal for strained type II superlattice infrared detectors," *J. Appl. Phys*. **62**, 2545–2548 (1987).
73. B.F. Levine, "Quantum-well infrared photodetectors," *J. Appl. Phys.* **74**, R1–R81 (1993).
74. A. Rogalski, "Quantum well photoconductors in infrared detectors technology," *J. Appl. Phys.* **93**, 4355–4391 (2003).
75. H. Schneider and H. C. Liu, *Quantum Well Infrared Photodetectors,* Springer, Berlin, 2007.
76. M. Zandian, J.D. Garnett, R.E. DeWames, M. Carmody, J.G. Pasko, M. Farris, C.A. Cabelli, D.E. Cooper, G. Hildebrandt, J. Chow, J.M. Arias, K. Vural, and D.N.B. Hall, "Mid-wavelength infrared p-on-on $Hg_{1-x}Cd_xTe$ heterostructure detectors: 30–120 Kelvin state-of-the-art performance," *J. Electron. Mater.* **32**, 803–809 (2003).
77. A. Rogalski and R. Ciupa, "Performance limitation of short wavelength infrared InGaAs and HgCdTe photodiodes," *J. Electron. Mater.* **28**, 630–636 (1999).
78. M.Z. Tidrow, W.A. Beck, W.W. Clark, H.K. Pollehn, J.W. Little, N.K. Dhar, P.R. Leavitt, S.W. Kennerly, D.W. Beekman, A.C. Goldberg, and W.R. Dyer, "Device physics and focal plane applications of QWIP and MCT," *Opto-Electron. Rev.* **7**, 283–296 (1999).
79. Y. Wei and M. Razeghi, "Modeling of type-II InAs/GaSb superlattices using an empirical tight-binding method and interface engineering," *Phys. Rev.* **B69**, 085316 (2004).
80. A. Rogalski, "Hg-based alternatives to MCT," in *Infrared Detectors and Emitters: Materials and Devices,* pp. 377–400, edited by P. Capper and C.T. Elliott, Kluwer Academic Publishers, Boston, 2001.
81. M.J. E. Golay, "A pneumatic infrared detector," *Rev. Sci. Instr.* **18**, 357–362 (1947).
82. E.M. Wormser, "Properties of thermistor infrared detectors," *J. Opt. Soc. Amer.* **43**, 15–21 (1953).
83. R. W. Astheimer, "Thermistor infrared detectors," *Proc. SPIE* **443**, 95–109 (1983).
84. G.W. McDaniel and D.Z. Robinson, "Thermal imaging by means of the evaporograph," *Appl. Opt.* **1**, 311–324 (1962).

85. C. Hilsum and W.R. Harding, "The theory of thermal imaging, and its application to the absorption-edge image tube," *Infrared Phys.* **1**, 67–93 (1961).
86. A.J. Goss, "The pyroelectric vidicon – A review," *Proc. SPIE* **807**, 25–32 (1987).
87. R. A. Wood and N. A. Foss, "Micromachined bolometer arrays achieve low-cost imaging," *Laser Focus World*, 101–106 (June, 1993).
88. http://www.flir.com/uploadedFiles/Eurasia/Cores_and_Components/Technical_Notes/uncooled%20detectors%20 BST.pdf
89. T. Schimert, C. Hanson , J. Brady, T. Fagan, M. Taylor, W. McCardel, R. Gooch, M. Gohlke, and A.J. Syllaios, "Advances in small pixel, large format á-Si bolometer arrays," *Proc. SPIE* **7298**, 72980T-1–5 (2009).
90. JJ. Yon, JP. Nieto, L. Vandroux, P. Imperinetti, E. Rolland, V. Goudon, C. Vialle, and A. Arnaud, "Low resistance α-SiGe based microbolometer pixel for future smart IR FPA," *Proc. SPIE* **7660**, 76600U-1–7 (2010).
91. C. Hanson, "IR detectors: amorphous-silicon bolometers could surpass IR focal-plane technologies," *Laser Focus Word*, April 1, 2011.
92. N. Roxhed, F. Niklaus, A.C. Fischer, F. Forsberg, L. Höglund, P. Ericsson, B. Samel, S. Wissmar, A. Elfvingc, T.I. Simonsen, K. Wang, and N. Hoivik, "Low-cost uncooled microbolometers for thermal imaging," *Proc. SPIE* **7726**, 772611-1–10 (2010).
93. *Seeing Photons: Progress and Limits of Visible and Infared Sensor Arrays*, Committee on Developments in Detector Technologies; National Research Council, 2010, http://www.nap.edu/catalog/12896.html
94. P. Norton, "Detector focal plane array technology", in *Encyclopedia of Optical Engineering*, edited by R. Driggers, pp. 320–348, Marcel Dekker Inc., New York, 2003.
95. R. Thom, "High density infrared detector arrays," U.S. Patent No. 4,039,833 (1977).
96. A.S. Gilmore, "High-definition infrared FPAs," *Raytheon Technology Today*, issue 1 (2008).
97. G. Destefanis, P. Tribolet, M. Vuillermet, and D.B. Lanfrey, "MCT IR detectors in France," *Proc. SPIE* **8012**, 801235-1–12 (2011)
98. A. Hoffman, "Semiconductor processing technology improves resolution of infrared arrays," *Laser Focus World*, 81–84, February 2006.
99. J.W. Beletic, R. Blank, D. Gulbransen, D. Lee, M. Loose, E.C. Piquette, T. Sprafke, W.E. Tennant, M. Zandian, and J. Zino, "Teledyne Imaging Sensors: Infrared imaging technologies for astronomy & civil space," *Proc. SPIE* **7021**, 70210H (2008).
100. A.M. Fowler, D. Bass, J. Heynssens, I. Gatley, F.J. Vrba, H.D. Ables, A. Hoffman, M. Smith, and J. Woolaway, "Next generation in InSb arrays: ALADDIN, the 1024×1024 InSb focal plane array readout evaluation results," *Proc. SPIE* **2268**, 340–345 (1994).
101. E. Beuville, D. Acton, E. Corrales, J. Drab, A. Levy, M. Merrill, R. Peralta, and W. Ritchie, "High performance large infrared and visible astronomy arrays for low background applications: Instruments performance data and future developments at Raytheon," *Proc. SPIE* **6660**, 66600B (2007).
102. A.W. Hoffman, E. Corrales, P.J. Love, and J. Rosbeck, M. Merrill, A. Fowler, and C. McMurtry, "2K×2K InSb for astronomy," *Proc. SPIE* **5499**, 59–67 (2004).
103. M.E. Ressler, H. Cho, R.A.M. Lee, K.G. Sukhatme, J.J. Drab, G. Domingo, M.E. McKelvey, R.E. McMurray, Jr., and J.L. Dotson, "Performance of the JWST/MIRI Si:As detectors," *Proc. SPIE* **7021**, 70210O (2008).
104. A. Rogalski, J. Antoszewski, and L. Faraone, "Third-generation infrared photodetector arrays," *J. Appl. Phys.* **105**, 091101 (2009).
105. D.F. King, J.S. Graham, A.M. Kennedy, R.N. Mullins, J.C. McQuitty, W.A. Radford, T.J. Kostrzewa, E.A. Patten, T.F. Mc Ewan, J.G. Vodicka, and J.J. Wootana, "3rd-generation MW/LWIR sensor engine for advanced tactical systems," *Proc.* **6940**, 69402R (2008).
106. S. Gunapala, S.V. Bandara, J.K. Liu, J.M. Mumolo, D.Z. Ting, C.J. Hill, J. Nguyen, B. Simolon, J. Woolaway, S.C. Wang, W. Li, P.D. LeVan, and M.Z. Tidrow, "Demonstration of megapixel dual-band QWIP focal plane array," *IEEE J. Quantum. Electron.* **46**, 285–293 (2010).
107. S.D. Gunapala, S.V. Bandara, J.K. Liu, E.M. Luong, S.B. Rafol, J.M. Mumolo, D.Z. Ting, J.J. Bock, M.E. Ressler, M.W. Werner, P.D. LeVan, R. Chehayeb, C.A. Kukkonen, M. Ley, P. LeVan, and M.A. Fauci, "Recent developments and applications of quantum well infrared photodetector focal plane arrays," *Opto-Electron. Rev.* **8**, 150–163 (2001).
108. A. Rogalski, "New material systems for third generation infrared photodetectors," *Opto-Electron. Rev.* **16**, 458–482 (2008).
109. R. Rehm, M. Walther, J. Schmitz, F. Rutz, A. Wörl, R. Scheibner, and J. Ziegler, "Type-II superlattices: the Fraunhofer perspective," *Proc. SPIE* **7660**, 76601G-1–12 (2010).
110. "Uncooled infrared imaging market commercial & military applications," *Market & Technology Report* – available in JULY 2011, Yole Development.
111. http://www.sofradir-ec.com/wp-uncooled-detectors-achieve.asp
112. S.H. Black, T. Sessler, E. Gordon, R. Kraft, T Kocian, M. Lamb, R. Williams, and T. Yang, "Uncooled detector development at Raytheon," *Proc. SPIE* **8012**, 80121A-1–12 (2011).
113. P. Martyniuk and A. Rogalski, "Quantum-dot infrared photodetectors: Status and outlook," *Prog. Quantum Electron.* **32**, 89–120 (2008).

